

## RESEARCH ARTICLE

# Deficiency of Tet3 in nucleus accumbens enhances fear generalization and anxiety-like behaviors in mice

Bu-Fang Fan<sup>1</sup>  | Bo Hao<sup>1,2</sup>  | Yun-Da Dai<sup>1</sup> | Li Xue<sup>3</sup>  | Yan-Wei Shi<sup>1,2</sup>  | Lu Liu<sup>1</sup>  | Shou-Min Xuan<sup>1</sup>  | Ning Yang<sup>1</sup>  | Xiao-Guang Wang<sup>1,2</sup>  | Hu Zhao<sup>1,2</sup> 

<sup>1</sup>Faculty of Forensic Medicine, Guangdong Province Translational Forensic Medicine Engineering Technology Research Center, Zhongshan School of Medicine, Sun Yat-sen University, Guangzhou, Guangdong, China

<sup>2</sup>Guangdong Province Key Laboratory of Brain Function and Disease, Zhongshan School of Medicine, Sun Yat-sen University, Guangzhou, Guangdong, China

<sup>3</sup>Department of Psychology, School of Public Medicine, Southern Medical University, Guangzhou, China

## Correspondence

Hu Zhao and Xiao-Guang Wang, Faculty of Forensic Medicine, Guangdong Province Translational Forensic Medicine Engineering Technology Research Center, Zhongshan School of Medicine, Sun Yat-sen University, Guangzhou, Guangdong, China.  
Email: zhaohu3@mail.sysu.edu.cn and wxguang@mail.sysu.edu.cn

## Funding information

National Natural Science Foundation of China, Grant/Award Numbers: 81530061, 81471829, 81273350; Natural Science Foundation of Guangdong Province, China, Grant/Award Numbers: 2022A1515012090, 2021A1515012471

## Abstract

Stress-induced neuroepigenetic programming gains growing more and more interest in the studies of the etiology of posttraumatic stress disorder (PTSD). However, seldom attention is focused on DNA demethylation in fear memory generalization, which is the core characteristic of PTSD. Here, we show that ten-eleven translocation protein 3 (TET3), the most abundant DNA demethylation enzyme of the TET family in neurons, senses environmental stress and bridges neuroplasticity with behavioral adaptation during fear generalization. Foot shock strength dependently induces fear generalization and TET3 expression in nucleus accumbens (NAc) in mice. Inhibition of DNA demethylation by infusing demethyltransferase inhibitors or AAV-Tet3-shRNA virus in NAc enhances the fear generalization and anxiety-like behavior. Furthermore, TET3 knockdown impairs the dendritic spine density, PSD length, and thickness of neurons, decreases DNA hydroxymethylation (5hmC), reduces the expression of synaptic plasticity-related genes including *Homer1*, *Cdkn1a*, *Cdh8*, *Vamp8*, *Reln*, *Bdnf*, while surprisingly increases immune-related genes *Stat1*, *B2m*, *H2-Q7*, *H2-M2*, *C3*, *Cd68* shown by RNA-seq. Notably, knockdown of TET3 in NAc activates microglia and CD39-P2Y12R signaling pathway, and inhibition of CD39 reverses the effects of TET3 knockdown on the fear memory generalization and anxiety. Overexpression of TET3 by Crispr-dSaCas9 virus delivery to activate endogenous Tet3 in NAc increases dendritic spine density of neurons in NAc and reverses fear memory generalization and anxiety-like behavior in mice. These results suggest that TET3 modulates fear generalization and anxiety via regulating synaptic plasticity and CD39 signaling pathway.

## KEYWORDS

CD39, fear generalization, nucleus accumbens (NAc), synaptic plasticity, ten-eleven translocation protein 3 (TET3)

## 1 | INTRODUCTION

Fear memories imprinted by traumatic stress are critical for survival. However, excessive generalization of fear, characterized not only by a strong response to a previously learned threatening cue, but also a debilitating

Bu-Fang Fan and Bo Hao contributed equally to this study.

This is an open access article under the terms of the [Creative Commons Attribution-NonCommercial-NoDerivs](https://creativecommons.org/licenses/by-nc-nd/4.0/) License, which permits use and distribution in any medium, provided the original work is properly cited, the use is non-commercial and no modifications or adaptations are made.

© 2022 The Authors. *Brain Pathology* published by John Wiley & Sons Ltd on behalf of International Society of Neuropathology.

failure to suppress fear responses even from cues that are neutral or signal safety, is one of the hallmarks of anxiety and stress-related disorders. The fear generalization contributes to intrusion (re-experiencing the fear response in safe situations), avoidance (avoiding trauma-related stimuli), and hyperarousal (abnormal vigilance and reactivity), all of which are core symptoms of posttraumatic stress disorder (PTSD) [1, 2]. Tremendous fear responses in nonhazardous situations bring in huge psychological burdens, encumbering life passions [3].

The prevalence of PTSD is about 8% in the general population, but much higher in a certain population with high trauma exposure. It is found that in combat-exposed veterans and rape victims, the PTSD prevalence reaches up to 25% [4] and 50% [5], respectively. Notably, 80% of the holocaust survivors suffered intrusive recollections, and 90% endured recurrent nightmares [6]. Unfortunately, current treatment for PTSD is far from satisfactory, and the neurobiology of PTSD needs to be clarified to address the reported “PTSD pharmacotherapy crisis” [7]. However, animal models of PTSD with high transferability are still a challenge to meet.

Because PTSD is precipitated by definite traumatic stress, fear conditioning is commonly used as animal models of PTSD. Classical fear conditioning model induced by mild or moderate stress show adaptive reactions in normal fear learning, while the fear generalization models induced by more intense stress exposure are better able to reproduce core PTSD symptoms [5]. In contrast to the classical fear conditioning model, which focuses primarily on quantitative aspects of fear memories such as freezing levels in response to a conditioned stimulus (CS+), the fear generalization models focus on maladaptive fear response to both CS+ and unpaired neutral stimulus (CS−). The fear generalization models gain increasing interest in PTSD research, while the molecular encoding of stressful experiences and the neural mechanisms of fear generalization remain to be explored.

Epigenetic mechanisms incorporate individual experiences and trauma exposure into the genetic background to elicit a spectrum of fear responses [7, 8]. Traumatic load of variability in nature and degree would result in specific epigenetic modifications. DNA methylation and demethylation are important epigenetic modifications modulating gene expression. In terminally differentiated cells such as neurons, DNA methylation has long been considered as a permanent repressive epigenetic mark until recent reports show that postmitotic neurons exhibit extensive DNA demethylation [9, 10]. DNA methylation and demethylation are dynamically regulated in fear learning and memory [8, 11].

The ten-eleven translocation (TET) family is found to be essential in converting 5-methylcytosine (5mC) to 5-hydroxymethylcytosine (5hmC) [12]. The mammalian brain contains the highest 5hmC levels, and 5hmC accumulates across the lifespan [13], highlighting the critical role of TET in experience-induced epigenetic modification.

TET1 is identified to modulate negative mood diseases, including anxiety and depression [14, 15]. TET2 is important in accommodating the cognitive function of the hippocampus in mice [16]. TET3 is the most abundant enzyme of the family in the brain. Homozygous deletion of Tet3 has been demonstrated to result in neonatal lethality [17, 18]. The phenotypes of Tet3 deficiency in humans exhibit hypotonia, autism, facial dysmorphism, motion disorders, intellectual disability, and/or global developmental delay [19, 20]. Notedly, TET3 is identified as a synaptic sensor by regulating gene expression in response to global synaptic activity changes in hippocampal neurons [21]. Kremer et al. found that the expression of TET3, rather than TET1 or TET2, is increased in hippocampal neurons during contextual fear memory formation [22]. Importantly, fear extinction has been proven to cause the accumulation of 5hmC in the prefrontal cortex, which is dependent on the activity of TET3 [23]. Although growing evidence supports a functional role of TET3 in fear memory, the effect of TET3-dependent DNA demethylation on fear generalization has yet to be determined.

In this study, we aimed to explore the modulation of fear generalization by TET3 in nucleus accumbens (NAc), a key brain region interfacing limbic, cognitive and executive circuitry [24].

## 2 | MATERIALS AND METHODS

### 2.1 | Animals

C57BL/6 adult male mice weighing 22–30 g (8–12 weeks old) were fed in a temperature-controlled room ( $23 \pm 1^\circ\text{C}$ ) on a 14 h/10 h light/dark cycle. Animal experiments were conducted in accordance with the “Guidelines for the Care and Use of Laboratory Animals” issued by the National Institutes of Health (NIH) and approved by the Ethics Committee of Sun Yat-sen University School of Medicine, Sun Yat-sen University.

### 2.2 | Behavior test

#### 2.2.1 | Fear generalization

Fear generalization was performed as previously described [25, 26]. The experimental protocol was shown in Figure 1A. Two sets of contexts (A and B) with different lighting conditions, floors, walls, and odors were used. Antecedent to the start, all chambers were sterilized with 75% alcohol. On the floor of the conditioning chamber, the previously installed metal grids delivered foot shocks (US) (Context A: 12-in. wide  $\times$  10-in. deep  $\times$  12-in. high). In one group, subjects were randomly selected from different littermates. During the habituation session in Context A on Day 1, mice received five stimuli of either two auditory tones (total duration of 10 s, consisting of either 5-kHz

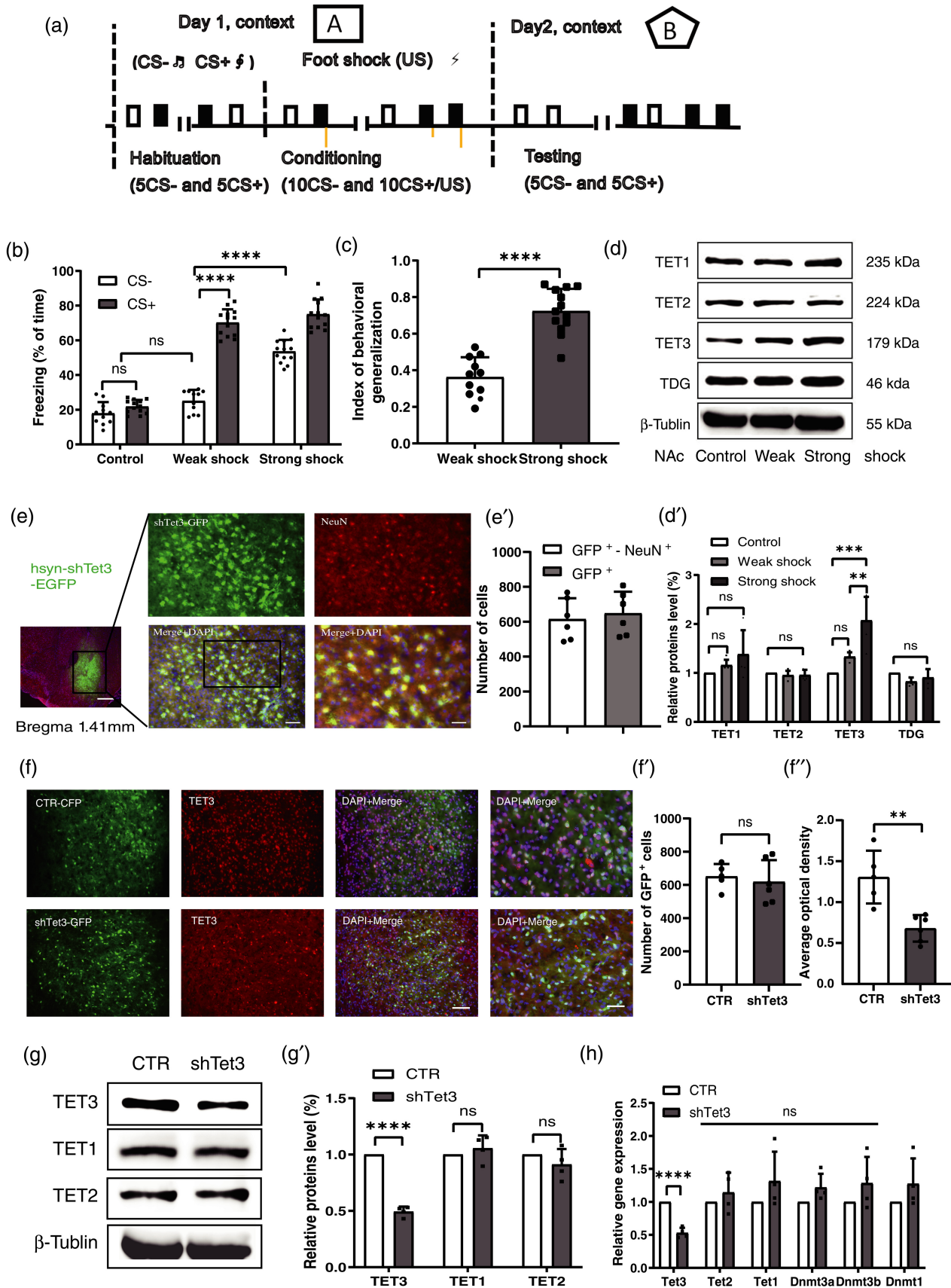


FIGURE 1 Legend on next page.

clicks repeated at 5 Hz [CS−] or continuous tones at 1 kHz [CS+], 5-ms rise and fall,  $70 \pm 5$  dB sound pressure level). Immediately after the habituation session, discriminative fear conditioning was performed where only CS+ of these two tones was paired (10 pairings, average intertrial interval  $\langle \text{ITI} \rangle = 70$  s, with a range of 40–100 s) with a 1-s scrambled foot shock (US) and was coterminated with the US. Ten CS+–US pairs were randomly matched with ten CS− pairs in an interleaved manner during conditioning. The frequencies used for the CS+ and CS− were counterbalanced across animals. The method of sound delivery was via a speaker (5  $\Omega$ ; Coulbourn Instruments) placed in the chamber. Status post 24 h on Day 2, the conditioned mice in context B were tested with both CS− and CS+ (10 s, five trials each,  $\langle \text{ITI} \rangle = 70$  s, 40–100 s). The magnitude of their freezing levels in response to the two tones represented the extent of recalling fear memory. The index of behavioral generalization (IBG) was measured as the ratio of average freezing response of CS− to CS+ in the testing session.

### 2.2.2 | Open field

Each mouse was placed in the center of the chamber with free motion and video recording. A significantly more time was used for them to explore the peripheral area in a manner of physically contacting the walls than to explore the open central area. Locomotor activity was analyzed to measure the total distance traveled and time used. The subjects that spent significantly less time in the open central area were deemed to demonstrate anxiety-like behavior [27].

### 2.2.3 | Elevated plus maze

The elevated plus maze was set with two installed interleaved open and closed arms, lifting 4 ft off the ground. Mice were placed in the center. The time spent in open arms was recorded by Ethovision tracking software, lasting 5 min in total [27].

### 2.2.4 | Sucrose preference

A single housed mouse was first fed with two bottles of water for 1 day, followed by three consecutive days with one bottle of water and another one of 1% sucrose. The amount of consumption in each bottle was tracked, after which the two bottles were switched and the volumes were recorded again [27].

### 2.2.5 | Tail suspension test

Each mouse was hung upside down on the stand by a rubber rope tied about 2 cm from the tip of the tail. The head was about 15 cm above the floor. Immobility time was recorded by video and we calculated the total immobility time within 6 min [28].

## 2.3 | Drugs infusion

A concentration of 3 mg/kg solution was made by dissolving and diluting 1,5-isoquinolinediol with saline. It was then injected via an intraperitoneal pathway for 4 h before the behavioral test [29]. For CD39 inhibitor administration, Guide cannulas (62001; RWD Life Science) were implanted bilaterally in the NAc (+1.41 mm A/P, +0.75 mm M/L,  $\pm 4.70$  mm D/V from Bregma), the coordinate was based on the latest mouse brain atlas [30], and fixed to the skull with dental cement after viral injection. After 7 days of recovery, mice received three consecutive days of CD39 inhibitor ARL67156 [31] before behavioral tests.

## 2.4 | Western blot

Immediately after the behavior test, the brains of subjects were removed after euthanasia, and NAc tissues were taken within 1-mm diameter of the coordinate (+1.41 mm A/P, +0.75 mm M/L,  $\pm 4.70$  mm D/V from Bregma) point were collected. We homogenized samples

**FIGURE 1** Foot shock strength dependently induces fear memory generalization with TET3 expression in NAc and knockdown of TET3 in NAc with TET1 and TET2 unaffected. (A) Experimental protocol. Day 1, tone-habituation and conditioning. Day 2, testing. CS, 10 s; US, 1 s; average intertrial interval ( $\langle \text{ITI} \rangle = 70$  s (40–100 s). (B) The histogram represents freezing % to CS− and CS+ in no shock group ( $n = 11$ ), weak shock group ( $n = 13$ ), and strong shock group ( $n = 13$ ). (C) The histogram represents the index behavior of generalization (IBG) of the three groups, IBG was calculated by the ratio of the freezing % of CS− to CS+ (no shock group:  $N = 11$ , weak shock group:  $N = 13$ , strong shock group:  $N = 13$ ). (D and D') Western blotting shows the levels of TET1, TET2, TET3, and TDG in NAc of the control group, weak shock group, and strong shock group. Data are standardized to the control group ( $n = 4$ , from 8 mice, each sample in triplicate). (E) Immunofluorescence micrographs of the AAV virus injection site. Scale bars = 200  $\mu\text{m}$ . Immunofluorescence micrographs of colabeling of GFP<sup>+</sup> cells and NeuN<sup>+</sup> neurons. Scale bars = 100  $\mu\text{m}$  (left), 50  $\mu\text{m}$  (right). (E') The number of GFP<sup>+</sup> – NeuN<sup>+</sup> cells and GFP<sup>+</sup> cells. The percentage of colabeling cells is about 95.38% ( $n = 6$  images per mice,  $n = 6$ ). (F) Immunofluorescence micrographs of CTR ( $n = 5$ ) and shTet3 group ( $n = 6$ ). Scale bars = 100  $\mu\text{m}$  (left), 50  $\mu\text{m}$  (right). Six micrographs for each mouse. DAPI, 4',6-diamidino-2-phenylindole. (F') Quantification of GFP<sup>+</sup> cells in NAc from CTR mice and shTet3 mice. (F'') Quantification of the TET3<sup>+</sup> cell average optical density in NAc. (G and G') Western blotting shows the levels of TET3, TET1, and TET2 expression in CTR and shTet3 group ( $n = 4$ , from eight mice, each sample in triplicate). (H) Quantitative PCR for mRNA expression of Tet1, Tet2, Dnmt3a, Dnmt3b, and Dnmt1. Data are standardized to the CTR group ( $n = 4$ , from 12 mice, each sample in triplicate). Quantifications are presented as means  $\pm$  SEM. (B) Two-way ANOVA with Tukey's test; (C, F', F'', G, and H) Unpaired two-tailed *t*-test; (D') One-way ANOVA with Tukey's test; \*\* $p < 0.01$ , \*\*\* $p < 0.001$ , \*\*\*\* $p < 0.0001$ ; ns, not significant

in RIPA buffer (Beyotime Biotechnology) containing 1 mM protease inhibitor PMSF (Beyotime Biotechnology). Proteins were resolved in 8% acrylamide sodium dodecyl sulfate–polyacrylamide gel electrophoresis and transferred to a polyvinylidene difluoride membrane (Immobilon-P; Millipore). Blots were incubated overnight at 4°C in a mixed solution with rabbit polyclonal anti-TET3 (1:1000; Catalog# ab139311; Abcam), anti-TET1 (1:1000; Catalog# ab191698; Abcam), anti-TET2 (1:1000; Catalog# ab94580; Abcam), anti-TDG (1:1000; Catalog# ab154192; Abcam), and other antibodies (see Table S1). Bands were amplified with horseradish peroxidase-conjugated secondary antibodies (1:2000; Catalog# 7074s; Cell Signaling Technology). The visualization of the membrane was achieved by X-ray film exposure (ECL kit; Thermo Fisher Scientific). The target protein immunoreactivity was normalized to GAPDH (1:1000; Catalog# 2118s; Cell Signaling Technology) or  $\beta$ -tubulin (1:1000; Catalog# 2146s; Cell Signaling).

## 2.5 | Stereotaxic surgery

Before the start, subjects undertook sodium pentobarbital anesthesia (40 mg/kg, intraperitoneal injection). Wuhan BrainVTA Viral Biotechnology Company supplies all the vector viruses. To knock down Tet3, three interference shRNA sequences of targeted Tet3 (sh1, sh2, sh3) were designed under the instruction of the online design software of Thermo Fisher website, and the sh2 was found to be most effective. The sh2 short-hairpin sequence was shown as the following: 5'-CTGTC TCAGATACAGATATGG-3'. Both the specificity and efficiency of the shRNA were validated. The high titers of engineered rAAV-hsyn-EGFP-5'miR-30a-shRNA(Tet3)- miR30a-3'-WPRE-pA (shTet3), type 9 or rAAV-hsyn-EGFP-5'miR-30a-shRNA (scramble)-3'- miR30a-wpres (CTR), type 9 were infused bilaterally into the NAc (+1.41 mm A/P, +0.75 mm M/L,  $\pm$ 4.70 mm D/V from Bregma), the coordinate was based on the latest mouse brain atlas [30]) prepared subjects at a rate of 300 nl/min to reach a total of 300 nl per side. Sufficient diffusion of viruses was ensured by leaving the steel needle in place for an additional 5 min status postinjection. Eye drops were applied to prevent dryness. Behavioral assays were performed 3 weeks later and the brains of all subjects were examined to confirm the accuracy of injection sites at the end of the experiments. For Tet3 overexpression, we used Crispr-dSaCas9 to activate endogenous Tet3 transcription, sasgRNAs were designed on an online website, and sequences with significant cleavage efficiency sasgRNA were screened for plasmid packaging. Efficiency sasgRNA as follows: LV-0341, LV-U6-sgRNA7(Tet3)-CMV-SV40; NLS-SaCas9-NLS-Flag-P2A-Puro-T2A-EGFP-WPRE; (Antisense: CTGGAGCTCTGGTTCTCCAAG). LV-CMV-SV40NLS-dSaCas9-HA-2XSV40NLS-VPR-EF1 $\alpha$ -Puro-T2A-EGFP-U6-SasgRNA (BbsI)-WPRE (CTR), LV-CMV-SV40NLS-dSaCas9-HA-2XSV40NLS-VPR-

EF1 $\alpha$ -Puro-T2A-EGFP-U6-SasgRNA (Tet3)-WPR (OE-Tet3) were infused bilaterally into the NAc of aforementioned prepared mice at a rate of 300 nl/min to reach a total amount of 800 nl per side, and behavioral assays were performed 10 days after viral injection.

## 2.6 | Quantification of 5hmC and 5mC

The global level of 5hmC and 5mC were assessed by Epi-Quik Hydroxymethylated DNA Immunoprecipitation (hMeDIP) Kit (Epigentek, P-1038) and MethylFlash Methylated DNA Quantification Kit (Epigentek, P-1034) after DNA extraction from mice NAc, which tissues were taken within 1-mm diameter of the coordinate (+1.41 mm A/P, +0.75 mm M/L,  $\pm$ 4.70 mm D/V from Bregma) point in accordance with the manufacturer's instructions.

## 2.7 | RNA-sequencing and genome-wide transcriptome analysis

The selections of RNA for sequencing targeted on samples from brain NAc were taken within 1 mm diameter of the coordinate (+1.41 mm A/P, +0.75 mm M/L,  $\pm$ 4.70 mm D/V from Bregma) point in CTR, shTet3, shocked CTR, and shocked shTet3 (three biological replicates for each group). After initial preparation, the RNA-seq experiments were carried out in Novogene (Beijing). Brief descriptions are as below: status post-RNA isolation from fresh NAc tissues by using TRIzol (Invitrogen), mRNA was purified by applying poly-T oligo-attached magnetic beads. Sequencing libraries were generated from NEBNext UltraTM RNA Library Prep Kit for Illumina (NEB) per the manufacturer's recommendations; and the index codes were added to attribute sequences to every sample. As the library generation was completed, initial quantification of samples was performed using Qubit2.0 Fluorometer and the solution was diluted to 1.5 ng/ $\mu$ l. Agilent 2100 bioanalyzer proceeded to detect the insert size of the library. The quality of the library was guaranteed by ensuring the accuracy of qRT-PCR quantification till the effective library concentration (higher than 2 nM). Once the preparations passed quality inspection, they were sequenced on an Illumina Hisq platform and 150 bp paired-end reads were generated. Raw data (raw reads) in fast-q format was first processed through in-house Perl scripts. Clean data (clean reads) was obtained by removing reads containing adapters, frames including poly-N and low-quality fragments. Criteria for analysis of gene differential expressions are as below:  $|\log_2(\text{FoldChange})| \geq 1$  and  $p \text{ adj} \leq 0.05$ . The FPKM values of genes were analyzed by mainstream hierarchical clustering, and rows (row) were calibrated for normalization (Z-score). Gene ontology (GO) functional and

Kyoto Encyclopedia of Genes and Genomes (KEGG) pathway enrichment of differential gene sets were performed in cluster profile software,  $p$  adj smaller than 0.05 was considered to be significant.

## 2.8 | RNA isolation and qPCR

The NAc tissues, which were taken within 1 mm diameter of the coordinate (+1.41 mm A/P, +0.75 mm M/L,  $\pm 4.70$  mm D/V from Bregma) point, was dissected and HP Total RNA Kit (R6812-01 OMEGA bio-tek) was used for the extraction and purification of RNA. The measurement was done on a Nanodrop spectrophotometer. Next, reverse transcription was conducted with the Transcriptor cDNA Synth. Kit 2 (Roche). Real-time qPCR was performed with LightCycler 480 SYBR Green I Master (Roche) and we exerted the  $\Delta\Delta C_t$  method to obtain relative fold change of expression in comparison with control samples, followed by the Gapdh process for normalization. Complete information about primers is listed in Table S2.

## 2.9 | Immunofluorescence analysis of mouse brain sections

Mice were sedated with sodium amobarbital (40 mg/kg, i.p.) in advance; thereafter, cold 0.9% saline and then 4% paraformaldehyde were perfused transcardially. Status post the resection of brain tissues, the samples were put in 4% paraformaldehyde overnight for fixation, and then they were transferred into phosphate-buffered saline (PBS) containing 30% sucrose until them sank to the bottom of 15 ml centrifuge tubes. The samples were dissected into 20- $\mu$ m sections by frozen slicer (CM1850, Leica, Germany) and were mounted on poly-L-lysine-coated slides for immunofluorescence detection. The blockage occurred in PBS containing 3% BSA, Goat serum, and 0.2% Triton X-100 for 2 h at room temperature. The sections were labeled by fluorescent secondary antibodies for 2 h at room temperature in incubation. Nuclei were counterstained using DAPI (1:5000; Sigma) for 8 min at room temperature and covered with slip dipped in ProLong Gold anti-fade reagent (Thermo Fisher Scientific). We used Olympus Fluoview FV1000 confocal microscope (Olympus) to acquire fluorescence images; the analysis of average optical density proceeded using the ImageJ software, while FIJI software ran the count of double-positive cells (three sections per animal and three subjects per group). To quantify total cell populations in the NAc (TET3<sup>+</sup> cells–NeuN<sup>+</sup> cells and GFP<sup>+</sup>–NeuN<sup>+</sup> cells), every sixth section (20- $\mu$ m thick) of the brain containing NAc was selected and immunostained. The total numbers of positive cells in all slices per animal were multiplied by six to estimate the number of cells per NAc. The percentage of colabeling cells is

calculated by the ratio of the number of colabeling cells to the total number of TET3<sup>+</sup> cells or GFP<sup>+</sup> cells.

## 2.10 | Golgi–Cox staining and image analysis

Golgi–Cox staining was performed using an FD Rapid Golgi Stain Kit (FD Neurotechnologies) [32]. Following euthanasia and dissection, the obtained brain tissues were impregnated in equal volumes of Solution A and B containing mercuric chloride, potassium dichromate, and potassium chromate, after which they were in storage at room temperature for 14 days. For every 24 h, the impregnation solution was replaced. On Day 15, the brain samples were transferred into Solution C and in storage at 4°C for 48 h while replacing the solution every 24 h as above described. Prior to mounting the sliced sections on gelatin-coated microscope slides with Solution C and staining, sagittal dissection in cryogenic surroundings was used to achieve a thickness of 100  $\mu$ m.

Only the impregnated neurons from the NAc were selected for dendrite analysis. As a prerequisite, the dendrite had to be intact and distinguishable from its neighboring neurons to avert mistracking. An upright microscope (BX63-1; Olympus Corporation) captured the Z-stack images of these neurons. The trace of dendrite branches was simulated by ImageJ software (NIH) with Neuron Jplugin [33], as well as the length, the number of dendritic branches, and spines. To analyze neuronal arborization, we counted the number of crossings from dendrites of concentric circles originating at the soma on ImageJ software (Sholl analysis plugin) [34].

## 2.11 | Electron microscope and quantification

Before dissecting the NAc of mice brains, mice were sedated with sodium pentobarbital (Nembutal; 45 mg/kg, i.p.) and perfused with 2% paraformaldehyde–2% glutaraldehyde (pH 7.4). The tissue samples were sliced to 1 mm<sup>3</sup> pieces in the same fixative; then in storage at 4°C overnight. Coronal dissection was selected to obtain 50- $\mu$ m thick slices. They were then postfixed with 1% osmium Tetroxide for 1 h. Sections were dehydrated in the ascending grades of ethanol (50%–75%–80%–95%–100%) for 10 min and embedded in Araldite mixture 60°C for 51 h. Small pieces of samples (approximately 1 mm<sup>3</sup>) were cut out of embedding sections. Presliced on an ultramicrotome and stained with Toluidine blue. The observation areas were determined by semithin sections (1  $\mu$ m). Ultrathin sections (70 nm) were stained with 4% uranyl acetate for 80 min and 0.4% lead citrate for 2 min under an electron microscope. Images were captured with a FEI (Tecnai G2 Spirit Twin) transmission electron microscope at a magnification of 13,500 and 37,000 times [35].

The density of synapses in various categories was quantified in terms of referred criteria [36]. To avoid

systematic sampling bias, we discarded areas containing large dendrites and somata. The identification and quantification of synapses were performed on ImageJ. Spine density was calculated as the number of the spine per  $\mu\text{m}^2$  ( $\times 13,500$  magnification, single image area =  $42.5 \mu\text{m}^2$ ). Enlargement of micrographs to a magnification of 37,000 times endorsed measurements of the average thickness of a PSD, its cytoplasmic outline, and peripheral dense materials. For each synapse, the thickness of the postsynaptic membrane is divided by its length to get an average thickness of PSD. Two investigators proceeded with all the measurements independently.

## 2.12 | Statistical analysis

The results are presented as mean  $\pm$  SEM and determined by unpaired two-tailed *t*-test for two-group comparisons or ANOVA followed by Turkey test for multiple comparisons among more than two groups. For experiments with two independent variables, two-way ANOVA followed by Tukey's or Šidák's multiple comparisons test was used. Data were considered significant as follows:  $*p < 0.05$ ,  $**p < 0.01$ ,  $***p < 0.001$ ,  $****p < 0.0001$ . All statistical analyses were carried out using SPSS 22.0 or GraphPad Prism 9.0. Test details are described in figure captions and Table S3.

## 3 | RESULTS

### 3.1 | Foot shock strength dependently induces fear generalization and TET3 expression in NAc

The risk of stress-related disorders is associated with the feature and severity of traumatic load. The fear memory induced by Pavlovian fear conditioning can be modulated by variation in the US itself [25]. The fear generalization model was performed as previously described [26]. Mice were first trained to discriminate between two tones with different frequencies: one (CS+) was paired with a foot shock (US) and the other was not (CS-) (Figure 1A). Animals were divided into three groups: the control group (without shock), the weak shock group (0.4 mA shock), and the strong shock group (1.2 mA shock). All mice conditioned with the weak shock and the strong shock showed conditioned fear memory as freezing behavior in response to CS+ significantly increased relative to the control group. However, mice receiving strong shock also showed fear memory generalization as the freezing behavior in response to CS- significantly increased compared with the control group (Figure 1B). Index behavior of generalization (IBG, the ratio of the freezing percentage of CS- to CS+) was applied to evaluate the fear memory generalization level. As shown in Figure 1C, the strong shock group exhibited a higher level than the weak shock group (Figure 1C).

To investigate the role of DNA demethylation in fear memory generalization, the expression of DNA demethyltransferases TET1, 2, 3, thymine DNA glycosylase (TDG) in NAc (Figure 1D) was examined by Western blot immediately after the retrieval test. It was found that only TET3 increased shock-intensity dependently, indicating that TET3 is the key DNA demethyltransferase in the regulation of fear memory generalization (Figure 1D'). The TET3 was highly colabeled with neuronal marker NeuN as shown by 99.47% of TET3<sup>+</sup> and NeuN<sup>+</sup> colabeling cells (Figure S1), which is consistent with previous studies showing that TET3 is highly expressed in the mature neurons of adult mouse brain [21, 23]. Taken together, these results indicate that the foot shock induces fear memory generalization and TET3 expression in NAc in an intensity-dependent manner.

### 3.2 | Knockdown of TET3 in NAc increases fear generalization

TET3 is required for neuronal development and differentiation [37, 38]. However, its functional roles in mature neurons are unclear. We hereby used shRNA interference technology to specify the role of Tet3 in fear memory generalization in adult mice. An AAV delivering shRNA targeted Tet3 (shTet3) was injected into the NAc of mice 3 weeks before the fear conditioning experiments. Three shRNA sequences, sh1, 2, and 3 were used, and the sh2 was the most effective (Figure S2). The colabeling of GFP with NeuN revealed that sh2 expression was neuron-specific (Figure 1E). The proportion of colabeling cells was about 95.38% (Figure 1E'). TET3 expression was reduced by 50% in the core and shell regions of NAc after 21 days of AAV injection (Figure 1E), whereas TET1 and 2 were unaffected (Figure 1F,G'), and the number of GFP<sup>+</sup> cells was not different between the CTR and shTet3 mice (Figure 1F'). Furthermore, qRT-PCR results confirmed that the mRNA expression levels of Tet1, Tet2, Dnmt3a, Dnmt3b, and Dnmt1 were unaffected (Figure 1H). The sh2 AAV was applied in the subsequent experiments. Mice with or without TET3 knockdown were conditioned with various intensities of foot shock: no shock (0 mA), weak shock (0.4 mA), moderate shock (0.8 mA), and strong shock group (1.2 mA). All mice were tested 24 h after fear conditioning. As the TET3 expression was stress dependently increased during fear memory generalization, we hypothesized that knocking down TET3 might reverse generalization induced by strong stress, but not as expected, shTet3 mice of the strong shock group showed no significant difference in fear memory generalization as the freezing percentages to CS- and the IBG values were similar to those without TET3 knockdown (CTR group) (Figure 2F,G). This may be potentially due to the ceiling effects of the strong shock. Further research showed that knockdown of TET3 significantly increased the fear generalization induced by moderate shock

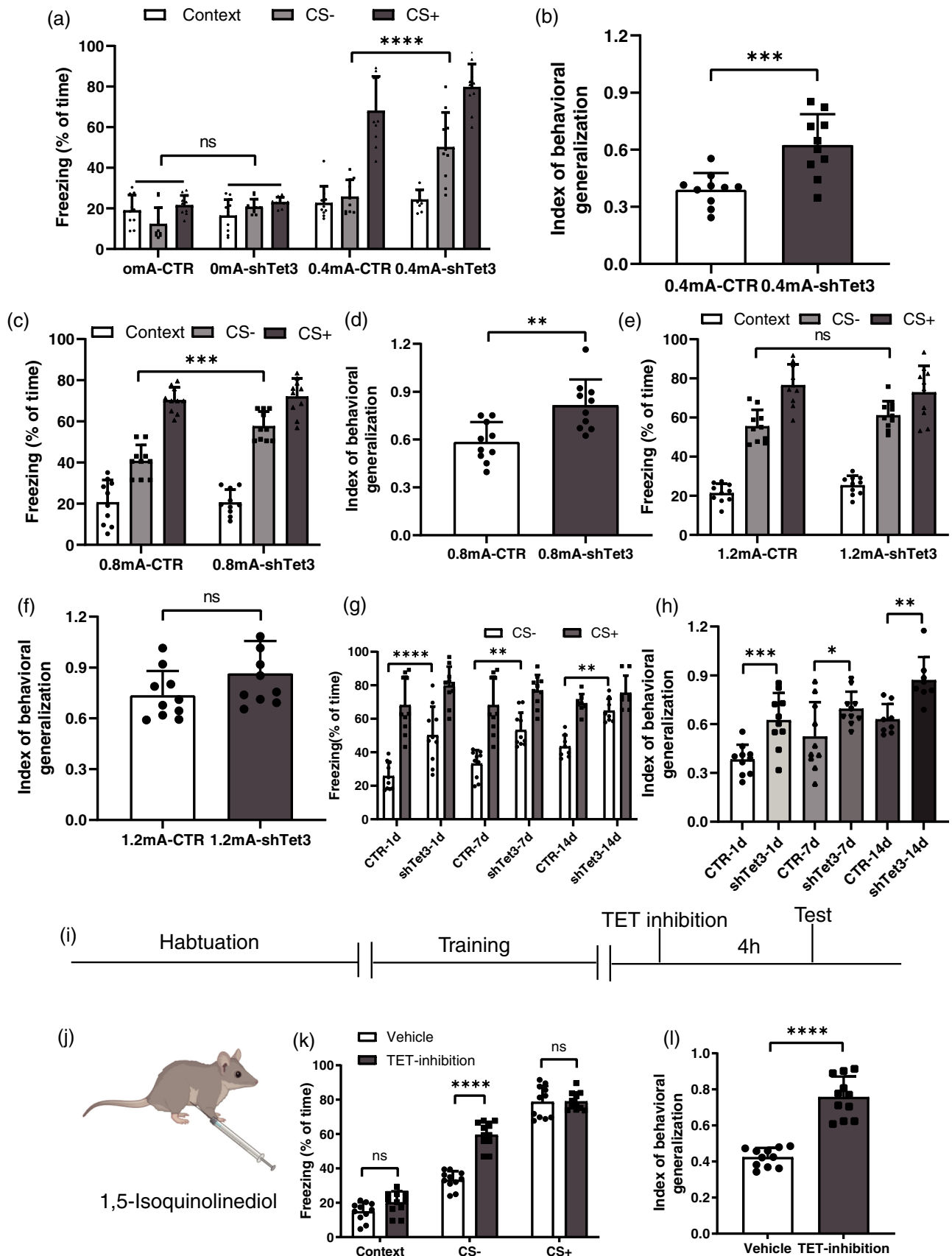


FIGURE 2 Legend on next page.



(Figure 2D,E). Notably, shTet3 mice in the weak shock group displayed significant fear memory generalization as shown by the significantly increased freezing percentages to CS- (Figure 2B) and IBG values relative to the control group (Figure 2C). In the baseline experiment, the mice without shock showed no significant difference in response to CS-, CS+, and the testing context between the CTR group and shTet3 group (Figure 2A). Since specific fear memory can generalize over time [39], the effect of TET3 knockdown on fear generalization was tested separately on the 1st, 7th, and 14th days after the fear conditioning. The shTet3 mice in the weak shock group also showed remarkable elevation in fear memory generalization on the 7th and 14th days compared with CTR mice (Figure 2H,I). These results implied that the knockdown of Tet3 could promote fear memory generalization for a long time. To assess whether the DNA demethylation is involved in fear memory generalization, we administrated 1,5-isoquinolinediol, a demethyltransferase inhibitor (Figure 2K), into the NAc 4 h prior (Figure 2J) to fear conditioning to inhibit the demethylation process [29]. The result revealed that inhibition of DNA demethylation facilitated fear memory generalization as the freezing behavior in response to CS- and IBG of the TET inhibition group (weak shock) was significantly higher than the vehicle group (Figure 2L,M).

In summary, these results suggest that either knockdown of TET3 or administration of TET inhibitor in NAc increases fear generalization.

### 3.3 | Knockdown of TET3 in NAc increases anxiety-like behavior

To investigate whether the knockdown of TET3 changed the spontaneous activity of mice, an open field experiment was conducted 3 weeks after the AAV injection. The results showed that knockdown of TET3 did not alter the total movement distances of mice (Figure 3A,B,E) but induced anxiety-like behavior as the central activity time and distance decreased (Figure 3A,C,D). Anxiety-like behavior was further confirmed by the elevated plus maze test. The shTet3 mice showed significantly reduced staying time in the open arms in contrast to the CTR group (Figure 3F,F'). The knockdown of

TET3 also caused a loss in the values of weight (Figure 3G,G'). In addition, we used tail suspension and sucrose preference experiments to exclude depression-like behaviors in shTet3 mice. The total immobility time and the percentage of sucrose preference were not significantly different between the two groups (Figure 3H,I). Altogether, these findings indicate that a lack of Tet3 in NAc increases anxiety-like behavior.

### 3.4 | Knockdown of TET3 induces differentially expressed synaptic plasticity-related and immune-related gene expression in NAc

Given that TET3 mediates the oxidization of 5mC into 5hmC [12], we speculated that the knockdown of TET3 would lead to the accumulation of 5mC in NAc via inhibiting DNA demethylation. To verify this hypothesis, the levels of 5hmC and 5mC in NAc tissues from the CTR and shTet3 groups were measured by using 5hmC and 5mC ELISA kit. As expected, TET3 knockdown resulted in a decrease in 5hmC, an increase in 5mC, and a decrease in the ratio of 5hmC to 5mC (Figure 4A), which is consistent with that reported previously in Tet1/3 RNAi knockdown mice [40].

To further clarify the mechanisms of transition from specific to generalized fear memory, QuantSeq 3'mRNA sequencing technology was applied to analyze transcripts RNA extracted from NAc tissues of the CTR and shTet3 mice with no shock (CTR and shTet3), or weak shock (S-CTR and S-shTet3). There were 1343 differential expressed transcripts in NAc of S-CTR (527 downregulated and 816 upregulated) compared with the CTR mice. In contrast, the differentially expressed transcripts in the S-shTet3 group increased up to 8772 (4190 downregulated and 4582 upregulated) in NAc compared with the S-CTR mice (Figure 4B). In the hierarchical clustering map of 52 representative differential expressed genes (DEGs) among the four groups, red and blue colors indicated upregulated and downregulated genes, respectively (Figures 4C and S3). According to the GO analysis, upregulated DEGs (red) in the S-CTR group compared to the CTR group were enriched in multiple items related

**FIGURE 2** Knockdown of TET3 in NAc enhances fear memory generalization. (A, B, D, and F) The histogram represents freezing % to CS- and CS+ in the no shock group, weak shock group, moderate shock group, and strong shock group of CTR ( $n = 10$ ) and shTet3 ( $n = 10$ ). (C, E, G) The histogram represents the quantification of index behavior of generalization (IBG) in the weak shock group, moderate shock group, and strong shock group of CTR and shTet3 (each group,  $n = 10$ ). (H) The histogram represents freezing % to CS- and CS+ in CTR and shTet3 group under weak shock, respectively, in 1 day ( $n = 10$ ), 7 days ( $n = 10$ ), and 14 days ( $n = 8$ ) after fear training. (I) The histogram represents the quantification of the index behavior of generalization of CTR and shTet3 group under weak shock, respectively, in 1 day ( $n = 10$ ), 7 days ( $n = 10$ ), and 14 days ( $n = 8$ ) after fear training. (J) Flow chart of the TET-inhibitor administration in the fear generalization behavior. (K) Intraperitoneal injection of TET-inhibitor 1,5-isoquinolinediol. (L) The histogram represents freezing % to CS- and CS+ in the CTR group ( $n = 11$ ) and TET inhibition group ( $n = 11$ ). (M) The histogram represents the quantification of index behavior of generalization of CTR ( $n = 11$ ) and TET-inhibitor group ( $n = 11$ ). Quantifications are presented as means  $\pm$  SEM. (A, B, D, F, and L) Two-way ANOVA with Šidák's test; (I) two-way ANOVA with Tukey's test; (C, E, G, M) unpaired two-tailed  $t$ -test; (H) three-way ANOVA with Tukey's test; \* $p < 0.05$ , \*\* $p < 0.01$ , \*\*\* $p < 0.001$ , \*\*\*\* $p < 0.0001$ ; ns, not significant

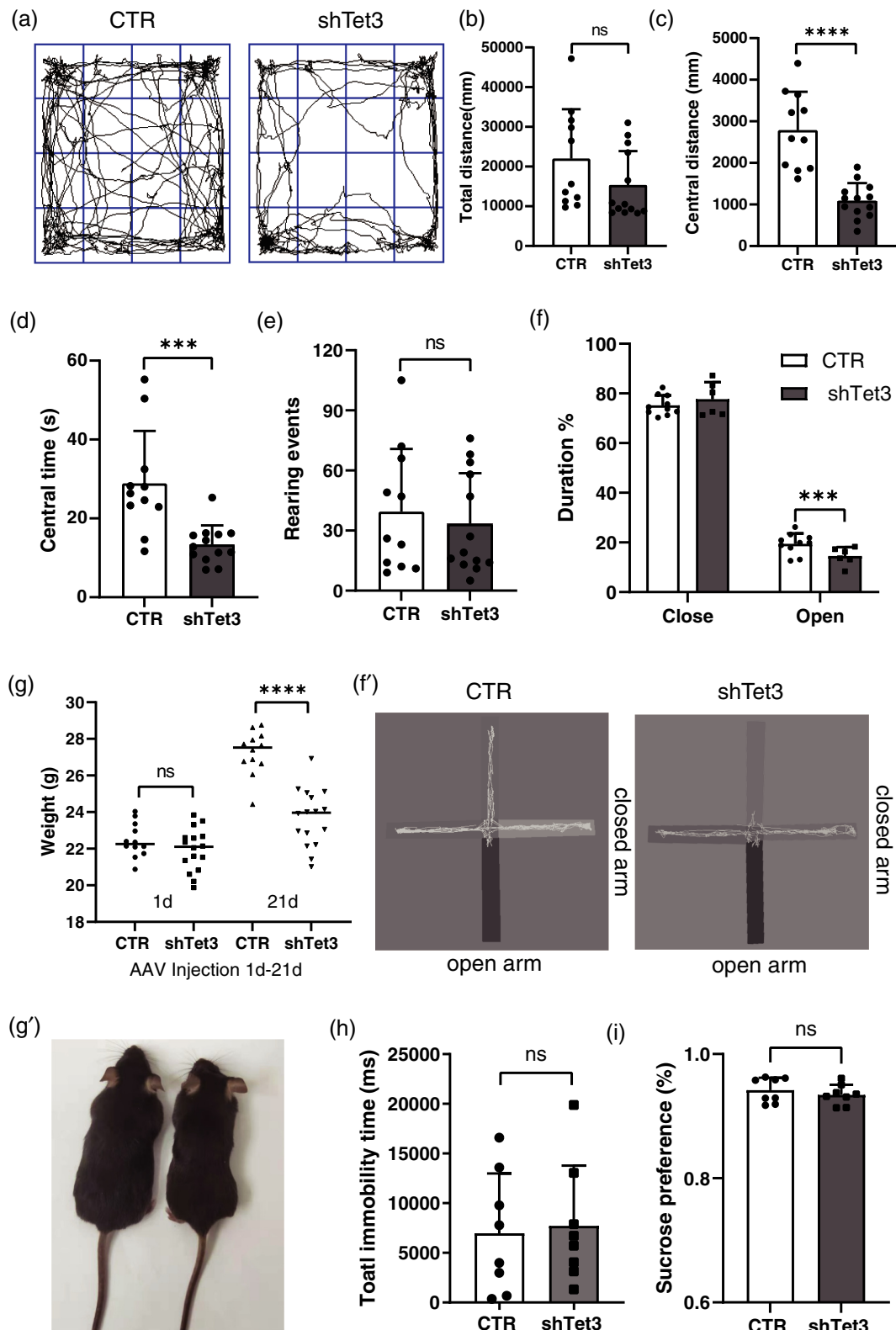


**FIGURE 3** Knockdown of TET3 in NAc enhances anxiety-like behaviors. (A–E) Open field test shows the central distance, total distance, central time, and rearing events of CTR group ( $n = 11$ ) and shTet3 group ( $n = 13$ ). (F and F') Elevated plus maze test shows the time in open arm and closed arm of CTR group ( $n = 8$ ) and shTet3 group ( $n = 8$ ). (G and G') The quantification of the weight in CTR ( $n = 12$ ) and shTet3 group ( $n = 16$ ) before and after AAV injection (21 days). (H) Tail suspension test shows the total immobility time of CTR ( $n = 8$ ) and shTet3 group ( $n = 8$ ). (I) Sucrose preference shows the percentage of sucrose preference of CTR ( $n = 8$ ) and shTet3 group ( $n = 8$ ). Quantifications are presented as means  $\pm$  SEM. (B, C, D, E, F, H, and I) Unpaired two-tailed  $t$ -test; (G) two-way ANOVA with Šidák's test; \*\* $p < 0.01$ , \*\*\* $p < 0.001$ , \*\*\*\* $p < 0.0001$ ; ns, not significant

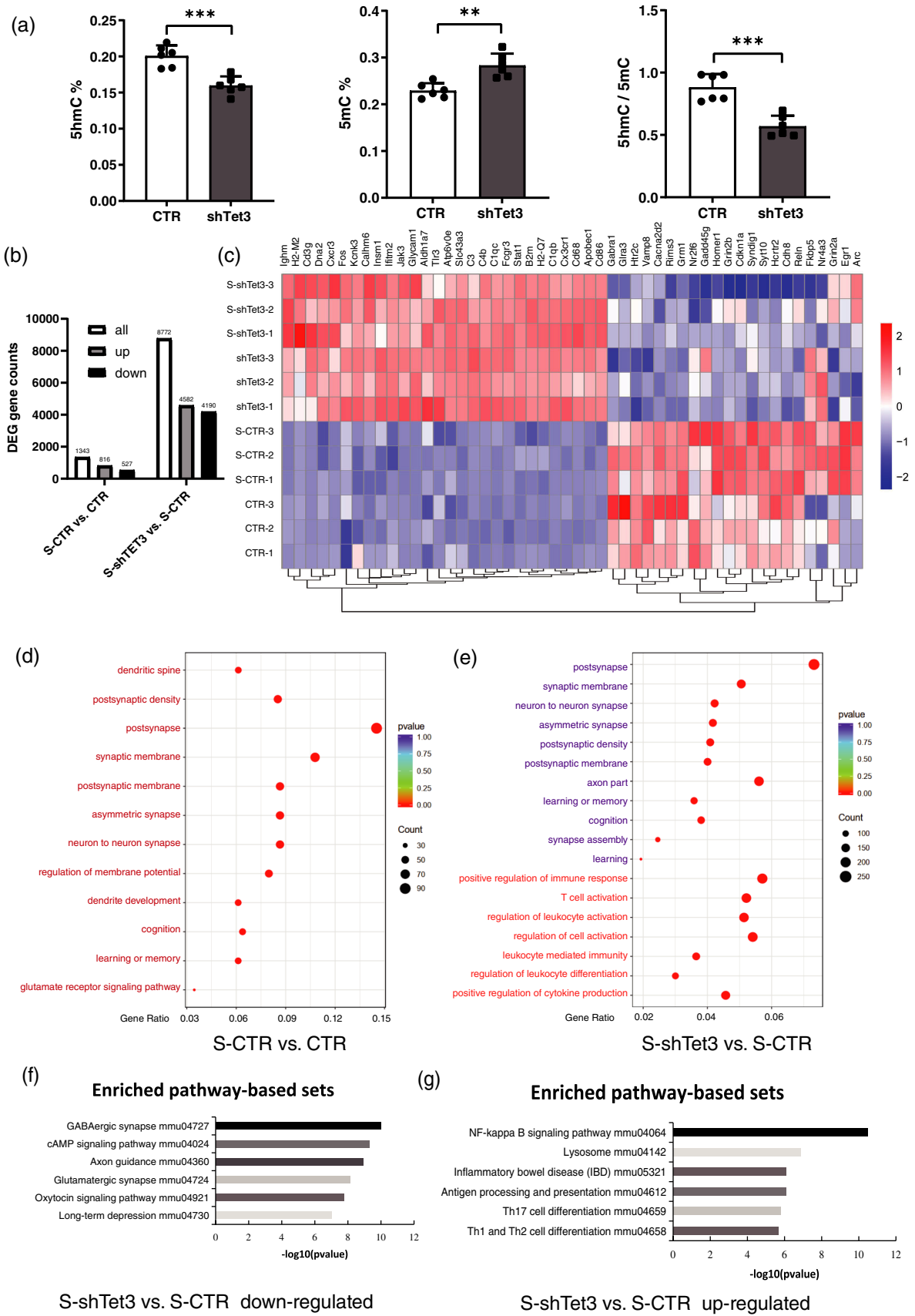


FIGURE 4 Legend on next page.

to synapse structure and function (Figure 4D), which indicates that fear learning altered synapse structure and function. In contrast, downregulated genes in the S-shTet3 group were significantly enriched in items related to synapse structure and synapse function (purple) compared to the S-CTR group, whereas upregulated genes were significantly enriched in items related to immune function (red) (Figure 4E). Moreover, the DEGs in the S-ShTet3 group compared to the shTet3 group were mainly enriched in respiratory chain complex, oxidoreductase complex, mitochondrial respiratory chain complex, NADH dehydrogenase complex, and Wnt-activated receptor activity (Figure S4), which are antioxidative and may promote cell survival [41]. Even though there was no difference in synaptic plasticity-related genes and immune-related genes between the S-shTet3 mice and shTet3 mice in NAc, antioxidative stress-related genes were increased in S-shTet3 mice compared to shTet3 mice.

Taken together, these GO enrichment results suggest that the knockdown of TET3 impairs fear learning via downregulating genes related to synapse structure and function, and activates the immune system.

Consistently, KEGG signaling pathway enrichment analysis revealed that GABAergic synapse (mmu04727), cAMP signaling pathway (mmu04024), axon guidance (mmu04360), glutamatergic synapse (mmu04724), and long-term depression (mmu04730) were down-enriched in the S-shTet3 mice relative to the S-CTR mice, which were antithesis in the S-CTR mice compared with the CTR mice (Figures 4F and S5). However, NF-kappa B signaling pathway (mmu04064) and lysosome (mmu04142) were up-enriched in the S-shTet3 mice relative to the S-CTR mice (Figure 4G). The mRNA levels of some down-regulated (*Homer1*, *Cdkn1a*, *Cdh8*, *Vamp8*, *Reln*, *Bdnf*, *Gadd45g*; Figure 5A) and upregulated genes (*Stat1*, *B2m*, *H2-Q7*, *H2-M2*, *C3*, *Cd68*, *Apobec1*; Figure 5B) from 52 DEGs were further validated by qRT-PCR. In addition, the downregulated genes also included synaptic-related genes such as *Dlg4*, *Sipall1*, *Synapsin1*, and *Grial* (Figure 5C). Meanwhile, immune-related genes *Tnf- $\alpha$* , *Anxa2*, *Thr8*, *Gusb*, and *Rpl13a* were upregulated (Figure 5D) in the shTet3 and S-shTet3 mice. The protein levels of Reelin, BDNF, and GluR1 were found to be consistent with the mRNA results (Figure S6). These findings demonstrate that the absence of TET3 induces differentially expressed synaptic plasticity-related and immune-related gene expression in NAc.

### 3.5 | Knockdown of TET3 impairs structural synaptic plasticity in NAc

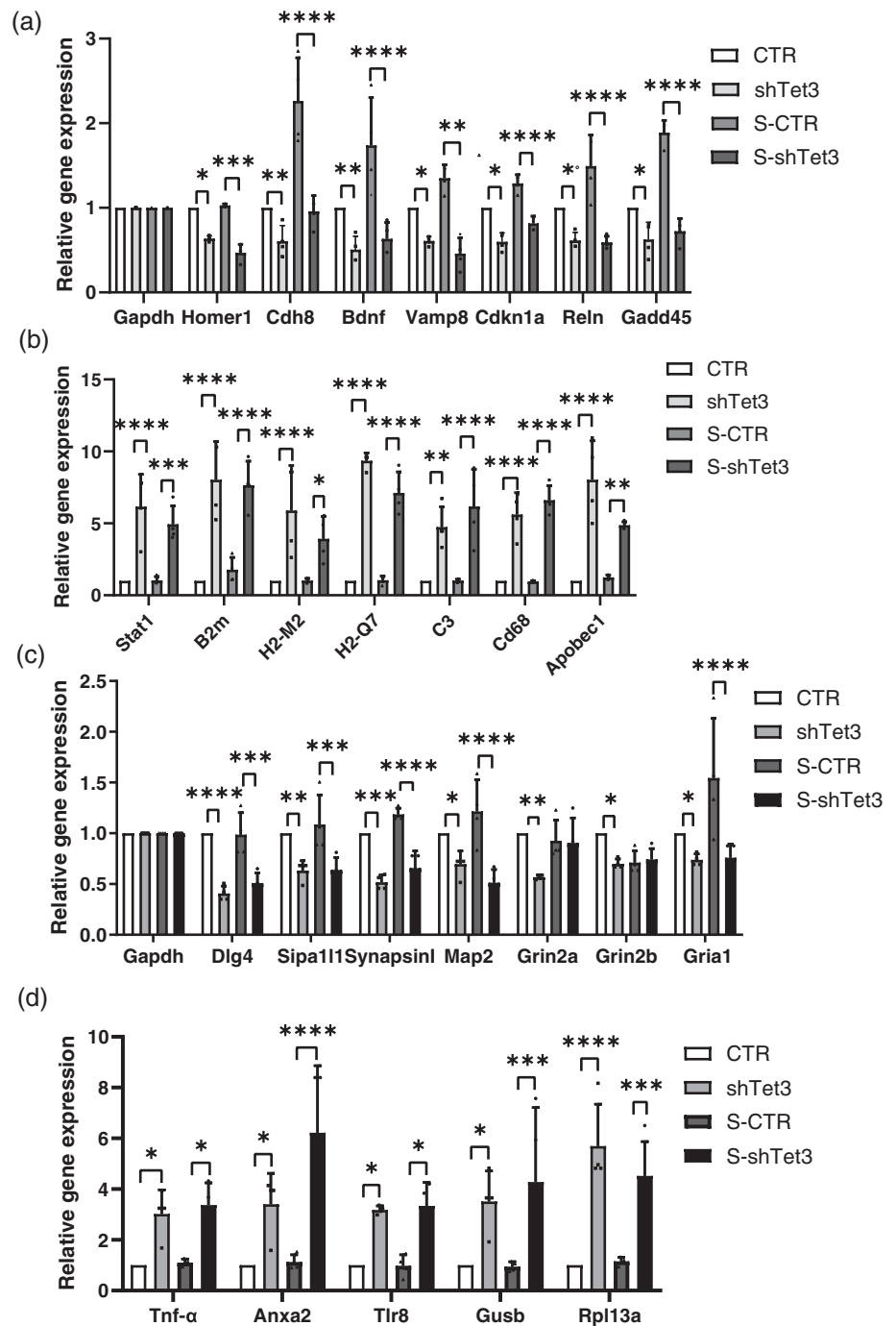
Considering the downregulation of synaptic genes in the TET3 knockdown mice, Golgi staining was performed to assess the effects of TET3 on neuronal morphology. S-shTet3 and shTet3 mice had fewer neuronal branches and shorter dendrites and displayed less complex neuron dendritic arborizations (Figure 6A). The total dendritic length and spine density of Golgi-stained neurons significantly declined in the shTet3 mice compared to the CTR mice, a similar result was observed in S-shTet3 mice compared with that in the S-CTR mice (Figure 6B–D). Consistent with the Golgi-staining data, electron microscopy (EM) analysis of total synapse density (including asymmetrical and symmetrical synapses) revealed significantly decreased densities in the shTet3 and S-shTet3 mice compared with their CTR groups (Figures 6E,F and S7). PSD length and thickness are used to evaluate the structure and function of the synapse. PSD length and thickness were reduced enormously in shTet3 and S-shTet3 mice compared with their CTR groups (Figure 6G,H), which indicates TET3 knockdown affects asymmetric synaptic plasticity and ultrastructural morphology.

### 3.6 | Knockdown of Tet3 activates microglia, and CD39 inhibitor reverses the fear memory generalization and anxiety-like behavior caused by knockdown of Tet3

As immune and inflammation-related genes were upregulated, and synaptic plasticity was downregulated in Tet3 knockdown mice, we speculated that knocking down TET3 in neurons may lead to excessive activation of peripheral microglia. To verify the hypothesis, immunofluorescence staining for microglia markers (Iba1) was conducted. It was found that the number of microglia in shTet3 mice was significantly increased compared with that in the control group. Notably, the microglia morphology has changed significantly (Figure 7A). It was reported that microglia respond to neuronal activation by suppressing neuronal activity, ATP was released by neurons and astrocytes upon neuronal activation, which triggers the recruitment of microglia protrusions. ATP was converted into AMP by the microglia ATP/ADP hydrolyzing ectoenzyme CD39, then AMP was converted

**FIGURE 4** Knockdown of TET3 in NAc induces decreased 5hmC and transcriptome analysis shows a predominant alteration in transcript levels of CTR, shTet3, shocked CTR (S-CTR), and shocked shTet3 (S-shTet3) mice in NAc. Gene expression analysis showed a decrease in the expression of synaptic plasticity regulated genes in shTet3 mice, and increased immunity regulated genes in shTet3 mice. (A) Enzyme-linked immunosorbent assay to detect the level of 5hmC and 5mC in NAc of CTR and shTet3 group ( $n = 6$ , each sample in triplicate). (B) The number of differentially expressed genes (DEGs; upregulated and downregulated) in the S-CTR versus CTR and S-shTet3 versus shTet3. (C) Hierarchical clustering of 52 DEGs in the CTR, shTet3, S-CTR, and S-shTet3. The red and blue colors indicate upregulated and downregulated genes, respectively. (D and E) Enriched gene ontology classes of differentially expressed targets in NAc of S-CTR versus CTR and S-shTet3 versus S-CTR. (F and G) enriched signaling pathways of DEGs in NAc of S-shTet3 versus S-CTR. Quantifications are presented as means  $\pm$  SEM. (A) Unpaired two-tailed  $t$ -test; \*\* $p < 0.01$ , \*\*\* $p < 0.001$

**FIGURE 5** Quantitative PCR examination of the expression of several DEGs of CTR, shTet3, S-CTR, and S-shTet3 mice in NAc. (A) Expression of synaptic-related genes *Homer1*, *cdk5*, *Cdh8*, *Vamp8*, *reelin*, *Bdnf*, *Gadd45g*, and so on were downregulated both in shTet3 and S-shTet3 mice. (B) Expression of immune-related genes *Stat1*, *B2m*, *H2-Q7*, *H2-M2*, *C3*, *Cd68*, and DNA demethylation gene *Apobec1* were upregulated both in shTet3 and S-shTet3 mice. (C) Expression of synaptic-related genes, *Dlg4*, *Sipa111*, *Synapsin1*, *Gria1* were downregulated in shTet3 mice and S-shTet3. *Grin2a* and *Grin2b* were downregulated only in shTet3. (D) Expression of immune-related genes, *Tnf- $\alpha$* , *Anxa2*, *Tlr8*, *Gusb*, *Rpl13a*, was upregulated in shTet3 mice both in the control and weak shock group. Each group  $n = 4$ , from 12 mice, each sample in triplicate. Quantifications are presented as means  $\pm$  SEM. (A–D) Two-way ANOVA with Tukey's test; \* $p < 0.05$ , \*\* $p < 0.01$ , \*\*\* $p < 0.001$ , \*\*\*\* $p < 0.0001$



into adenosine by CD73, and the adenosine mediated suppression of neuronal responses via the adenosine receptor A1R was essential for the regulation of neuronal activity and animal behavior [42]. We further performed qPCR and found that *Cd39*, *P2ry12*, and *Cd68* gene transcription were significantly enhanced in shTet3 mice compared with the control group (Figure 7B). Since CD39 is expressed only in microglia, CD73 is expressed in microglia as well as other brain cells, and constitutive deletion of CD39 can cause an inhibition of the microglia ramified phenotype in the brain with a reduction in the

length of processes, branching frequency and number of intersections with Sholl spheres [43], we further investigated whether inhibition of microglia CD39 can reverse fear memory generalization and anxiety-like behavior in shTet3 mice. The Tet3 knockdown AAV was injected into NAc of mice 21 days before drug administration through the cannulas fastened to the skull. shTet3 mice and control mice were administered either CD39 inhibitor or saline for continuously 3 days [31], then behavioral experiments were performed (Figure 7C). We found that CD39 inhibitor ARL67156 significantly reversed the fear

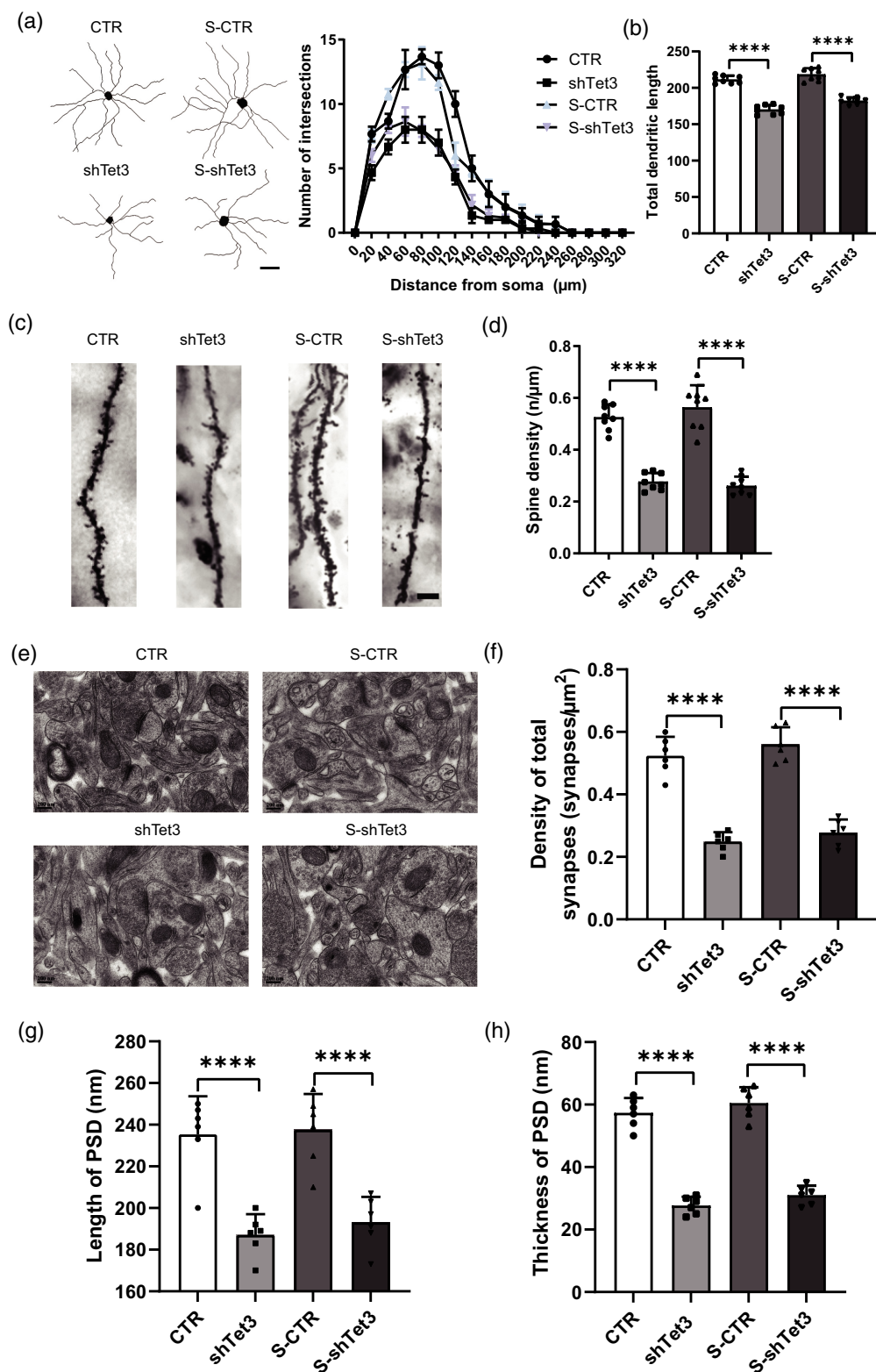


**FIGURE 6** Knockdown of TET3 impairs neuronal synaptic structural plasticity. (A) Reconstructions of Golgi-stained neurons in NAc. S-shTet3 and shTet3 mice had fewer neuronal branches and shorter dendrites and displayed less complex neuron dendritic arborizations compared to the CTR group ( $n = 8$  mice per group). Scale bar = 50  $\mu\text{m}$ . (B) Total dendritic length of reconstructed Golgi-stained NAc neuron ( $n = 20\text{--}25$  neurons per group,  $n = 8$  mice per group). (C) Micrographs of neuron dendrites from CTR, shTet3, S-CTR, and S-shTet3 group in NAc and bar graphs with quantification of spine density ( $n = 20\text{--}25$  neurons per group,  $n = 8$  mice per group) scale bar = 10  $\mu\text{m}$ . (D) Representative electron micrographs of synapses from CTR, shTet3, S-CTR, and S-shTet3 in NAc in high magnification. Scale bar = 200 nm. (E) Histogram plot of the density of total synapses, asymmetric synapses, and symmetric synapses ( $n = 50\text{--}55$  images per group,  $n = 6$  mice per group). (F and G) Histogram plot of the PSD length and PSD thickness ( $n = 50\text{--}55$  synapses per group,  $n = 6$  mice per group); ( $n = 50\text{--}55$  synapses per group,  $n = 6$  mice per group). Quantifications are presented as means  $\pm$  SEM. (A, B, D, F–H) two-way ANOVA with Tukey’s test; \*\*\* $p < 0.001$ , \*\*\*\* $p < 0.0001$ ; ns, not significant

memory generalization as shown by a significantly decreased freezing percentage to CS— as well as IBG value in shTet3 mice compared with the saline-shTet3 group (Figure 7D,E). In the open field test (Figure 7F), CD39 inhibitor also reduced anxiety-like behavior of the shTet3 mice with less central distances and time

(Figure 7G,I,J), while the total distance and rear events had no significant difference between the CD39 inhibitor groups and saline groups (Figure 7H,K). Moreover, Golgi staining of NAc neurons showed a significantly increased spine density in the CD39 inhibitor-shTet3 mice compared with saline-shTet3 mice (Figure S8).

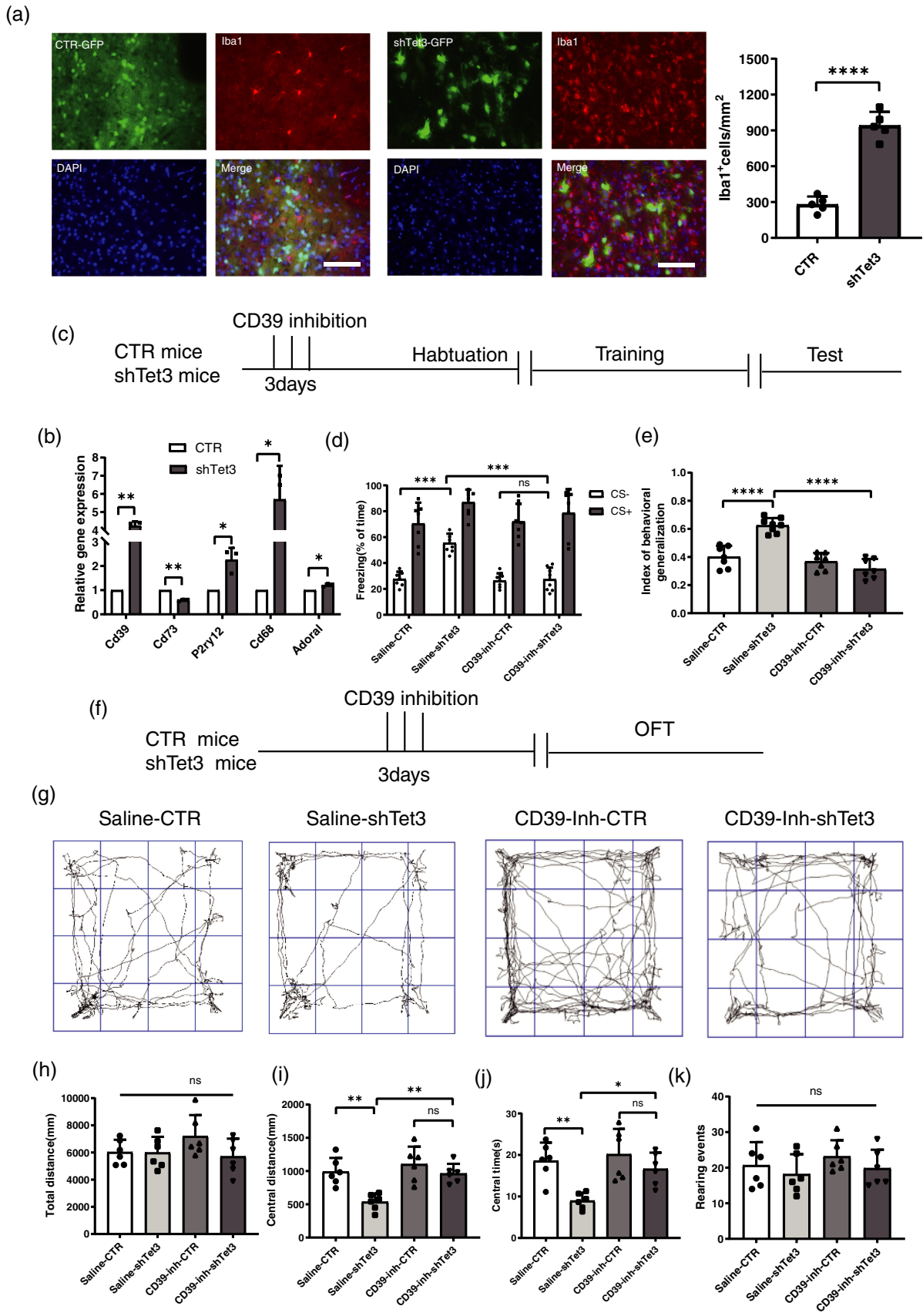


FIGURE 7 Legend on next page.

Altogether, these results indicate that deficiency of TET3 activates microglia, and CD39 inhibitor reverses the fear memory generalization and anxiety caused by knockdown of TET3.

### 3.7 | Overexpression of TET3 in the NAc reverses fear memory generalization and anxiety-like behavior

Finally, we tested whether TET3 overexpression could ameliorate fear generalization and anxiety-like behavior. Lentivirus conveyed Crispr-dSaCas9 to activate endogenous Tet3 transcription were injected in NAc. Immunofluorescence staining and Western blot showed that TET3 expression was substantially increased in the OE-Tet3 group (Figure 8A,B). Fear generalization behavior and open field tests were initiated 10 days after virus injection. Fear memory formation appeared to be unaffected with the weak shock (Figure 8C,D) between OE-Tet3 mice and CTR mice, while OE-Tet3 mice showed antifear generalization with the moderate shock (decreased freezing percentage to CS– as well as IBG value with moderate shock) compared to CTR mice (Figure 8E,F). In the open field test, the OE-Tet3 mice showed more central distances and time than the CTR mice (Figure 8G,I,J), but there was no significant difference in total distance and rear events (Figure 8G,H,K). Moreover, Golgi staining of NAc neurons showed increased spine density in the OE-Tet3 mice (Figure 8L, M). Altogether, these findings indicate that overexpression of TET3 in the NAc reverses fear memory generalization and anxiety-like behavior induced by stress.

## 4 | DISCUSSION

A growing body of data indicates that NAc, a rewarding hub [44] in the brain, plays an important role in several aversive learning behaviors [45–47]. A recent study supports the causal role of reduction of DNA methyltransferase DNMT3a in NAc of rats in PTSD-like behavior induced by predatory-associated “trauma” (cat scent) [48]. The present study improved our understanding of the role of TET3-dependent DNA demethylation

in NAc in fear generalization. Our data showed that foot shock strength dependently induced fear generalization and TET3 expression in NAc. Knockdown of TET3 in NAc increased the fear generalization induced by moderate stress. Notably, knockdown of TET3 even evoked the fear memory generalization in animals with mild stress exposure, where normally the animals never show maladaptive fear responses to neutral or safe cues. Potential reasons include reward processing and circuit dysregulation in the NAc of shTet3 mice when their capacities of prejudging risks drop in harsh environments, leading to fear memory generalization. Therefore, our results together with previous findings support the dynamic state of DNA methylation and demethylation in NAc as a target for the prevention and treatment of PTSD.

The discovery of the TET family of dioxygenases brings our understanding of DNA demethylation to a new height [49]. TET3 is highly expressed in mature neurons of the adult mouse brain [21, 23]. In our study, brain region-specific Tet3 knockdown was performed on NAc in adult mice and TET1 and TET2 escaped such deficiencies as previously reported in neural progenitor cells [50]. By knocking down TET3 expression, the level of 5hmC descended, as observed previously in Tet1/3 RNAi knockdown mice [40]. Knockdown of TET3 promoted both fear memory generalization and anxiety-like behavior. The extensive comorbidity of PTSD and anxiety disorder potentiates the likelihood that such knockdown of Tet3 might induce this phenomenon. Even though knockdown of TET1 in NAc induced anxiety-like behaviors [51, 52], TET1 overexpression in the hippocampal DG region is closely associated with anxiety-like behavior in mice [15]. A recent study concludes that conditional knockout of Tet3 in adult excitatory mature neurons in the hippocampus of adult mice increases anxiety-like behaviors [53]. It is highly implied that TET3 together with TET1 shares common characteristics of regulating anxiety-like behaviors through alternative pathways in the brain.

How TET3 modulates fear generalization and anxiety needs further exploration. Recently, it has been reported that acute stress produces enduring plasticity in NAc postsynapses and conditioned stress odors induce active behavioral coping strategies that are correlated with dendritic spine morphology [54]. In our study, knockdown of

**FIGURE 7** Knockdown of TET3 activates microglia, and CD39 inhibitor reverses the fear memory generalization and anxiety caused by knockdown of TET3. (A) Immunofluorescence micrographs and quantification of the number of Iba1<sup>+</sup> cells in NAc of CTR and shTet3 group (five to six micrographs for each mouse, each group,  $n = 5$ ). Scale bars = 50  $\mu\text{m}$ . (B) Quantitative PCR analysis of the expression of *CD39*, *P2Y12R*, *CD73*, *CD68*, and *A1R* gene expression in control and shTet3 mice ( $n = 5$ , from 15 mice, each sample in triplicate). (C) Flow chart of the CD39 administration in the fear generalization behavior. (D) The histogram represents freezing % to CS– and CS+ in saline and CD39-inhibitor group of CTR ( $n = 7$ ) and shTet3 mice ( $n = 7$ ). (E) The histogram represents the quantification of index behavior of generalization (IBG) in saline and CD39-inhibitor group of CTR ( $n = 7$ ) and shTet3 mice ( $n = 7$ ). (F) Flow chart of the CD39-inhibitor administration in the open field test. (G–K) Open field test depicts the central distance, total distance, central time, and rearing events in saline and CD39-inhibitor group of CTR and shTet3 mice (each group,  $n = 6$ ). Quantifications are presented as means  $\pm$  SEM. (A and B) Unpaired two-tailed  $t$ -test; (D) three-way ANOVA with Tukey’s test; (E, H–K) two-way ANOVA with Šidák’s test; \* $p < 0.05$ , \*\* $p < 0.01$ , \*\*\* $p < 0.001$ , \*\*\*\* $p < 0.0001$ ; ns, not significant



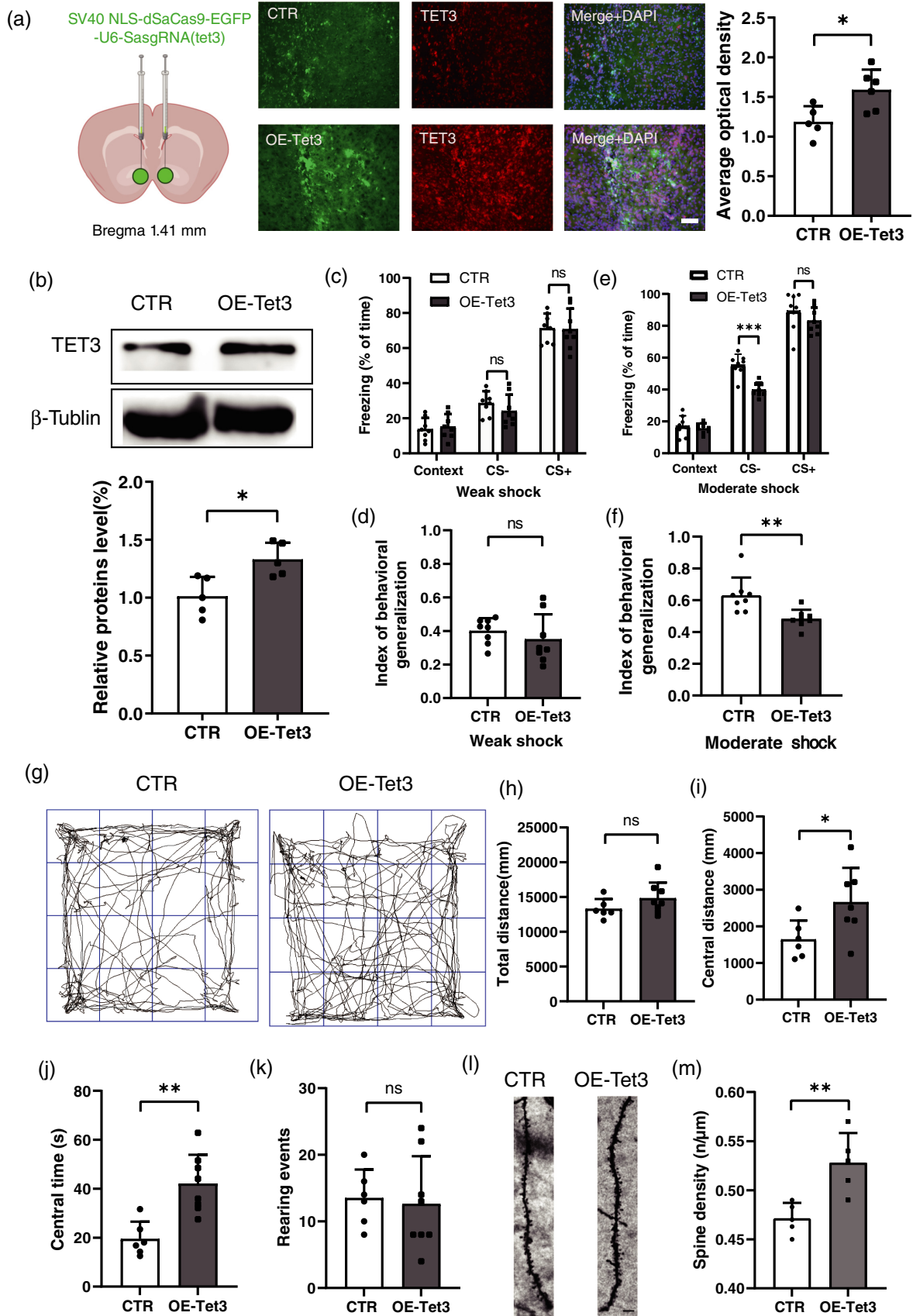


FIGURE 8 Legend on next page.

TET3 induced a downregulation on synaptic plasticity-related genes, inducing the transition from specific to generalized fear memory, which occurred in weak shock mice. Golgi staining and EM showed multiple damages to synaptic plasticity, suggesting that TET3 regulates the genes expression related to synaptic structure and function. On the other hand, knockdown of TET3 in cultured hippocampal neurons leads to excitatory transmission, which relies on the expression of GluR1 [21]. The inconsistency of our results with this conclusion might be since the fact that 90% of neurons in NAc are GABAergic [55], but those in the hippocampus and cortex are mostly excitatory neurons [56, 57]. TET3 may be dedicated to inhibitory signals in GABAergic neurons [58]. Another explanation is that in vivo neuronal TET3 knockdown is different from in vitro, considering in vivo neurons receive supportive connectivity from peripheral glial cells. The *Bdnf* gene promoter in TET3 knockdown neurons redounds to methylation and inhibits transcription [21]. The expressions of *Bdnf* and other synaptic-related genes are undermined inevitably while lacking TET3, which corresponds with our result that synaptic function-related genes *Bdnf*, *Dlg4* expression levels were significantly downregulated in Tet3 knockdown mice. We recently found that the GluN2B-BDNF signaling pathway plays an important role in fear generalization [26]. As BDNF is essential in maintaining synaptic function [59] and memory formation [60], its deficiency may exacerbate the disturbance of fear memory. Therefore, the impaired synaptic function of TET3 knockdown may be realized by mediating synaptic plasticity-related genes, such as *Bdnf*.

Our RNA-seq and qPCR analyses confirmed the distortion of immune gene expression in Tet3 knockdown mice. It is reported that Tet1 conditional knockout mice also show increased immune-related genes in NAc [14], and the dysregulation of immune gene expression is found during the process of fear memory formation [61–63]. Furthermore, we found knockdown of TET3 in NAc activated microglia and CD39-P2Y12R signaling pathway, and inhibition of CD39 reversed the fear memory generalization and anxiety caused by knocking down TET3 in NAc. Similarly, pharmacological inhibition and gene silencing of CD39 can increase the hippocampal neurogenesis and dendritic ridge density in mice accompanied by social frustration stress [31]. A

potential explanation points to the fact that knockdown of TET3 impairs the synaptic plasticity in neurons, which activates synapse repairing pathways by affecting cytokines signaling [64, 65], and microglia recruitment [66, 67]. It has been reported that microglia phagocytize synaptic components in the hippocampus of healthy adult mice, and the removal or inhibition of microglia phagocytosis by microglia prevents memory forgetting and dissociation of memory imprinted cells [66]. Together suggested that microglia may play a critical role in the generalization of fear memory through the remodeling of the synapse.

In our study, knockdown Tet3 mice also showed weight loss. The negative results from the sucrose preference test and tail suspension test indicate that depression is not the cause of weight loss in knockdown Tet3 mice. However, knockdown of TET3 enhanced anxiety, which may result in weight loss. It has been suggested that anxiety induced energy metabolism disorders, which cause weight loss [68]. Our study concentrated on the important role of TET3 in modulating fear memory generalization and anxiety-like behavior in male mice. One of the limitations of our study is female mice were not included. A large number of literature have shown that women are more vulnerable to stress- and fear-based disorders [69]. Since female mice had lower expression of TET enzyme than male mice in P25, and neonatal testosterone treatment of females could partially masculinize enzyme expression [70], the sex-specific function of TET3 in fear generalization and PTSD needs further exploration in the future.

In summary, our study supported a critical role of TET3-dependent DNA demethylation in NAc in the regulation of fear memory generalization. In the Tet3 knockdown mice, the downregulated synaptic plasticity-related genes and impaired synaptic structure suggested that TET3 owes its important role in regulating synaptic function. In the future, we will expect to delve into more genes that share interactions with TET3, the specific impact of TET3 in GABAergic subtypes and the precise mechanism of knockdown of TET3 induced microglial activation. The perspective of this research endorses our further understanding of the mechanism of PTSD and may propose new treatment strategies.

**FIGURE 8** Overexpression TET3 in NAc reverses fear memory generalization and anxiety-like behaviors with increased spine density. (A) Immunofluorescence micrographs and quantification of the TET3<sup>+</sup> cell average optical density in NAc of CTR ( $n = 5$ ) and OE-Tet3 ( $n = 6$ ) group (five to six micrographs for each mouse). Scale bar = 100  $\mu\text{m}$ . (B) Western blotting shows the levels of TET3 expression in CTR ( $n = 5$ , from 10 mice) and OE-Tet3 ( $n = 6$ , from 12 mice) group (each sample in triplicate). (C) The histogram represents freezing % to CS<sup>-</sup> and CS<sup>+</sup> in CTR and OE-Tet3 groups under weak shock (each group,  $n = 8$ ). (D) The histogram represents the quantification of index behavior of generalization (IBG) in CTR and OE-Tet3 group under weak shock (each group,  $n = 8$ ). (E) The histogram represents freezing % to CS<sup>-</sup> and CS<sup>+</sup> in CTR and OE-Tet3 groups under medium shock (each group,  $n = 8$ ). (F) The histogram represents the quantification of index behavior of generalization (IBG) in CTR and OE-Tet3 group under medium shock (each group,  $n = 8$ ). (G–K) Open filed test depicts the central distance, total distance, central time, and rearing events of CTR ( $n = 6$ ), and OE-Tet3 ( $n = 8$ ) mice. (L and M) Micrographs of neuron dendrites from CTR, OE-Tet3 group in NAc and bar graphs with quantification of spine density ( $n = 20$ – $25$  neurons per group,  $n = 8$  mice per group); scale bar = 10  $\mu\text{m}$ . Quantifications are presented as means  $\pm$  SEM. (C and E) Two-way ANOVA with Šidák's post hoc test; (A, B, D, F, H–K, M) unpaired two-tailed  $t$ -test; \* $p < 0.05$ , \*\* $p < 0.01$ ; \*\*\* $p < 0.001$ ; ns, not significant

## AUTHOR CONTRIBUTIONS

All authors had full access to all the data in the study and take responsibility for the integrity of the data and the accuracy of the data analysis. Hu Zhao, Xiao-Guang Wang, and Bu-Fang Fan conceived and planned the project; Bu-Fang Fan, Bo Hao, Yun-Da Dai, and Lu Liu performed the experiments; Bu-Fang Fan, Bo Hao, Shou-Min Xuan, Li Xue, and Yan-Wei Shi analyzed the data; Bu-Fang Fan, Ning-Yang, Xiao-Guang Wang and Hu Zhao wrote the manuscript; All authors discussed the results and commented on the manuscript. Hu Zhao supervised the project.

## ACKNOWLEDGMENTS

This work was supported by the National Natural Science Foundation of China (Grant no. 81530061, 81471829, and 81273350) and Project supported by the Natural Science Foundation of Guangdong Province, China (Grant no. 2022A1515012090, 2021A1515012471).



## CONFLICT OF INTEREST

The authors declare no conflicts of interest.

## DATA AVAILABILITY STATEMENT

The data that support the findings of this study are available from the corresponding author upon reasonable request.

## ORCID

Bu-Fang Fan  <https://orcid.org/0000-0002-5349-9947>  
 Bo Hao  <https://orcid.org/0000-0002-3410-2967>  
 Li Xue  <https://orcid.org/0000-0001-9939-9047>  
 Yan-Wei Shi  <https://orcid.org/0000-0001-5910-4822>  
 Lu Liu  <https://orcid.org/0000-0001-7772-0610>  
 Shou-Min Xuan  <https://orcid.org/0000-0001-5216-3758>  
 Ning Yang  <https://orcid.org/0000-0001-5756-8893>  
 Xiao-Guang Wang  <https://orcid.org/0000-0002-7598-1902>  
 Hu Zhao  <https://orcid.org/0000-0001-7971-0942>

## REFERENCES

- Dunsmoor JE, Paz R. Fear generalization and anxiety: behavioral and neural mechanisms. *Biol Psychiatry*. 2015;78(5):336–43.
- Laufer O, Israeli D, Paz R. Behavioral and neural mechanisms of overgeneralization in anxiety. *Curr Biol*. 2016;26(6):713–22.
- Duits P, Cath DC, Lissek S, Hox JJ, Hamm AO, Engelhard IM, et al. Updated meta-analysis of classical fear conditioning in the anxiety disorders. *Depress Anxiety*. 2015;32(4):239–53.
- Fulton JJ, Calhoun PS, Wagner HR, Schry AR, Hair LP, Feeling N, et al. The prevalence of posttraumatic stress disorder in operation enduring freedom/operation Iraqi freedom (OEF/OIF) veterans: a meta-analysis. *J Anxiety Disord*. 2015;31:98–107.
- Breslau N. Epidemiology of posttraumatic stress disorder in adults. In: Gayle Beck J, Sloan DM, editors. *The Oxford handbook of traumatic stress disorders*. New York, NY: Oxford University Press; 2012. p. 84–97.
- Kuch K, Cox BJ. Symptoms of PTSD in 124 survivors of the holocaust. *Am J Psychiatry*. 1992;149(3):337–40.
- Abdallah CG, Averill LA, Akiki TJ, Raza M, Averill CL, Gomaa H, et al. The neurobiology and pharmacotherapy of posttraumatic stress disorder. *Annu Rev Pharmacol Toxicol*. 2019;59:171–89.
- Zovkic IB, Sweatt JD. Epigenetic mechanisms in learned fear: implications for PTSD. *Neuropsychopharmacology*. 2013;38(1):77–93.
- Kriaucionis S, Heintz N. The nuclear DNA base 5-hydroxymethylcytosine is present in Purkinje neurons and the brain. *Science*. 2009;324(5929):929–30.
- Martinowich K, Hattori D, Wu H, Fouse S, He F, Hu Y, et al. DNA methylation-related chromatin remodeling in activity-dependent *BDNF* gene regulation. *Science*. 2003;302(5646):890–3.
- Bustos FJ, Ampuero E, Jury N, Aguilar R, Falahi F, Toledo J, et al. Epigenetic editing of the *Dlg4/PSD95* gene improves cognition in aged and Alzheimer's disease mice. *Brain*. 2017;140(12):3252–68.
- Ito S, Shen L, Dai Q, Wu SC, Collins LB, Swenberg JA, et al. Tet proteins can convert 5-methylcytosine to 5-formylcytosine and 5-carboxylcytosine. *Science*. 2011;333(6047):1300–3.
- Szulwach KE, Li X, Li Y, Song CX, Wu H, Dai Q, et al. 5-hmC-mediated epigenetic dynamics during postnatal neurodevelopment and aging. *Nat Neurosci*. 2011;14(12):1607–16.
- Feng J, Pena CJ, Purushothaman I, Engmann O, Walker D, Brown AN, et al. *Tet1* in nucleus accumbens opposes depression- and anxiety-like behaviors. *Neuropsychopharmacology*. 2017;42(8):1657–69.
- Kwon W, Kim HS, Jeong J, Sung Y, Choi M, Park S, et al. *Tet1* overexpression leads to anxiety-like behavior and enhanced fear memories via the activation of calcium-dependent cascade through *Egr1* expression in mice. *FASEB J*. 2018;32(1):390–403.
- Gontier G, Iyer M, Shea JM, Bieri G, Wheatley EG, Ramalho-Santos M, et al. *Tet2* rescues age-related regenerative decline and enhances cognitive function in the adult mouse brain. *Cell Rep*. 2018;22(8):1974–81.
- Gu TP, Guo F, Yang H, Wu HP, Xu GF, Liu W, et al. The role of *Tet3* DNA dioxygenase in epigenetic reprogramming by oocytes. *Nature*. 2011;477(7366):606–10.
- Tsukada Y, Akiyama T, Nakayama KI. Maternal *TET3* is dispensable for embryonic development but is required for neonatal growth. *Sci Rep*. 2015;5:15876.
- Beck DB, Petracovici A, He C, Moore HW, Louie RJ, Ansar M, et al. Delineation of a human mendelian disorder of the DNA demethylation machinery: *TET3* deficiency. *Am J Hum Genet*. 2020;106(2):234–45.
- Santos-Cortez RLP, Khan V, Khan FS, Mughal ZU, Chakchouk I, Lee K, et al. Novel candidate genes and variants underlying autosomal recessive neurodevelopmental disorders with intellectual disability. *Hum Genet*. 2018;137(9):735–52.
- Yu H, Su Y, Shin J, Zhong C, Guo JU, Weng YL, et al. *Tet3* regulates synaptic transmission and homeostatic plasticity via DNA oxidation and repair. *Nat Neurosci*. 2015;18(6):836–43.
- Kremer EA, Gaur N, Lee MA, Engmann O, Bohacek J, Mansuy IM. Interplay between TETs and microRNAs in the adult brain for memory formation. *Sci Rep*. 2018;8(1):1678.
- Li X, Wei W, Zhao QY, Widagdo J, Baker-Andresen D, Flavell CR, et al. Neocortical *Tet3*-mediated accumulation of 5-hydroxymethylcytosine promotes rapid behavioral adaptation. *Proc Natl Acad Sci U S A*. 2014;111(19):7120–5.
- Floresco SB. The nucleus accumbens: an interface between cognition, emotion, and action. *Annu Rev Psychol*. 2015;66:25–52.
- Ghosh S, Chattarji S. Neuronal encoding of the switch from specific to generalized fear. *Nat Neurosci*. 2015;18(1):112–20.
- Asim M, Hao B, Yang YH, Fan BF, Xue L, Shi YW, et al. Ketamine alleviates fear generalization through *GluN2B*-*BDNF* signaling in mice. *Neurosci Bull*. 2020;36(2):153–64.
- Krishnan V, Han MH, Graham DL, Berton O, Renthal W, Russo SJ, et al. Molecular adaptations underlying susceptibility and resistance to social defeat in brain reward regions. *Cell*. 2007;131(2):391–404.

28. Can A, Dao DT, Terrillion CE, Piantadosi SC, Bhat S, Gould TD. The tail suspension test. *J Vis Exp.* 2012;59:e3769.
29. Jayanthi S, Gonzalez B, McCoy MT, Ladenheim B, Bisagno V, Cadet JL. Methamphetamine induces TET1- and TET3-dependent DNA hydroxymethylation of *Crh* and *Ayp* genes in the rat nucleus accumbens. *Mol Neurobiol.* 2018;55(6):5154–66.
30. Franklin K, Paxinos G. The mouse brain in stereotaxic coordinates. 4th ed. New York, NY: Academic Press; 2012.
31. Cui QQ, Hu ZL, Hu YL, Chen X, Wang J, Mao L, et al. Hippocampal CD39/ENTPD1 promotes mouse depression-like behavior through hydrolyzing extracellular ATP. *EMBO Rep.* 2020;21(4):e47857.
32. Du F. Golgi-Cox staining of neuronal dendrites and dendritic spines with FD rapid GolgiStain™ kit. *Curr Protoc Neurosci.* 2019;88(1):e69.
33. Meijering E, Jacob M, Sarria JC, Steiner P, Hirling H, Unser M. Design and validation of a tool for neurite tracing and analysis in fluorescence microscopy images. *Cytometry A.* 2004;58(2):167–76.
34. Ferreira TA, Blackman AV, Oyrer J, Jayabal S, Chung AJ, Watt AJ, et al. Neuronal morphometry directly from bitmap images. *Nat Methods.* 2014;11(10):982–4.
35. Chen YF, Chen ZX, Wang RH, Shi YW, Xue L, Wang XG, et al. Knockdown of CLC-3 in the hippocampal CA1 impairs contextual fear memory. *Prog Neuropsychopharmacol Biol Psychiatry.* 2019;89:132–45.
36. Peters A, Palay SL, Webster H. The fine structure of the nervous system: neurons and their supporting cells. New York, NY: Oxford University Press; 1991.
37. Montalban-Loro R, Lozano-Urena A, Ito M, Krueger C, Reik W, Ferguson-Smith AC, et al. TET3 prevents terminal differentiation of adult NSCs by a non-catalytic action at *Snrpn*. *Nat Commun.* 2019;10(1):1726.
38. Xu Y, Xu C, Kato A, Tempel W, Abreu JG, Bian C, et al. Tet3 CXXC domain and dioxygenase activity cooperatively regulate key genes for *Xenopus* eye and neural development. *Cell.* 2012;151(6):1200–13.
39. Pollack GA, Bezek JL, Lee SH, Scarlata MJ, Weingast LT, Bergstrom HC. Cued fear memory generalization increases over time. *Learn Mem.* 2018;25(7):298–308.
40. Zhu X, Girardo D, Govek EE, John K, Mellén M, Tamayo P, et al. Role of Tet1/3 genes and chromatin remodeling genes in cerebellar circuit formation. *Neuron.* 2016;89(1):100–12.
41. Kawarada L, Fukaya M, Saito R, Kassai H, Sakagami H, Aiba A. Telencephalon-specific *Alkbh1* conditional knockout mice display hippocampal atrophy and impaired learning. *FEBS Lett.* 2021;595(12):1671–80.
42. Antonioli L, Pacher P, Vizi ES, Hasko G. CD39 and CD73 in immunity and inflammation. *Trends Mol Med.* 2013;19(6):355–67.
43. Matyash M, Zabiegalo O, Wendt S, Matyash V, Kettenmann H. The adenosine generating enzymes CD39/CD73 control microglial processes ramification in the mouse brain. *PLoS One.* 2017;12(4):e0175012.
44. LeGates TA, Kvarta MD, Tooley JR, Francis TC, Lobo MK, Creed MC, et al. Reward behaviour is regulated by the strength of hippocampus-nucleus accumbens synapses. *Nature.* 2018;564(7735):258–62.
45. Zhang Y, Zhu Y, Cao SX, Sun P, Yang JM, Xia YF, et al. MeCP2 in cholinergic interneurons of nucleus accumbens regulates fear learning. *Elife.* 2020;9:e55342.
46. Lemos JC, Wanat MJ, Smith JS, Reyes BA, Hollon NG, Van Bockstaele EJ, et al. Severe stress switches CRF action in the nucleus accumbens from appetitive to aversive. *Nature.* 2012;490(7420):402–6.
47. Reynolds SM, Berridge KC. Emotional environments retune the valence of appetitive versus fearful functions in nucleus accumbens. *Nat Neurosci.* 2008;11(4):423–5.
48. Warhaftig G, Zifman N, Sokolik CM, Massart R, Gabay O, Sapozhnikov D, et al. Reduction of *DNMT3a* and *RORA* in the nucleus accumbens plays a causal role in post-traumatic stress disorder-like behavior: reversal by combinatorial epigenetic therapy. *Mol Psychiatry.* 2021;26:7481–97.
49. Tahiliani M, Koh KP, Shen Y, Pastor WA, Bandukwala H, Brudno Y, et al. Conversion of 5-methylcytosine to 5-hydroxymethylcytosine in mammalian DNA by MLL partner TET1. *Science.* 2009;324(5929):930–5.
50. Santiago M, Antunes C, Guedes M, Iacovino M, Kyba M, Reik W, et al. *Tet3* regulates cellular identity and DNA methylation in neural progenitor cells. *Cell Mol Life Sci.* 2020;77(14):2871–83.
51. McMillan KA, Asmundson GJG. PTSD, social anxiety disorder, and trauma: an examination of the influence of trauma type on comorbidity using a nationally representative sample. *Psychiatry Res.* 2016;246:561–7.
52. Silove D, Momartin S, Marnane C, Steel Z, Manicavasagar V. Adult separation anxiety disorder among war-affected Bosnian refugees: comorbidity with PTSD and associations with dimensions of trauma. *J Trauma Stress.* 2010;23(1):169–72.
53. Antunes C, Da Silva JD, Guerra-Gomes S, Alves ND, Ferreira F, Loureiro-Campos E, et al. Tet3 ablation in adult brain neurons increases anxiety-like behavior and regulates cognitive function in mice. *Mol Psychiatry.* 2021;26(5):1445–57.
54. Garcia-Keller C, Carter JS, Krueger A, Kearns AM, Hopkins JL, Hodebourg R, et al. Behavioral and accumbens synaptic plasticity induced by cues associated with restraint stress. *Neuropsychopharmacology.* 2021;46(10):1848–56.
55. Francis TC, Lobo MK. Emerging role for nucleus accumbens medium spiny neuron subtypes in depression. *Biol Psychiatry.* 2017;81(8):645–53.
56. Banks PJ, Warburton EC, Bashir ZI. Plasticity in prefrontal cortex induced by coordinated synaptic transmission arising from reuniens/rhomboid nuclei and hippocampus. *Cereb Cortex Commun.* 2021;2(2):tgab029.
57. Liu Z, Wang Y, Cai L, Li Y, Chen B, Dong Y, et al. Prefrontal cortex to accumbens projections in sleep regulation of reward. *J Neurosci.* 2016;36(30):7897–910.
58. Wang L, Li MY, Qu C, Miao WY, Yin Q, Liao J, et al. CRISPR-Cas9-mediated genome editing in one blastomere of two-cell embryos reveals a novel Tet3 function in regulating neocortical development. *Cell Res.* 2017;27(6):815–29.
59. White AO, Kramár EA, López AJ, Kwapis JL, Doan J, Saldana D, et al. BDNF rescues BAF53b-dependent synaptic plasticity and cocaine-associated memory in the nucleus accumbens. *Nat Commun.* 2016;7:11725.
60. Lubin FD, Roth TL, Sweatt JD. Epigenetic regulation of *BDNF* gene transcription in the consolidation of fear memory. *J Neurosci.* 2008;28(42):10576–86.
61. Schubert I, Ahlbrand R, Winter A, Vollmer L, Lewkowich I, Sah R. Enhanced fear and altered neuronal activation in forebrain limbic regions of CX3CR1-deficient mice. *Brain Behav Immun.* 2018;68:34–43.
62. Enomoto S, Kato TA. Involvement of microglia in disturbed fear memory regulation: possible microglial contribution to the pathophysiology of posttraumatic stress disorder. *Neurochem Int.* 2021;142:104921.
63. Yu Z, Fukushima H, Ono C, Sakai M, Kasahara Y, Kikuchi Y, et al. Microglial production of TNF-alpha is a key element of sustained fear memory. *Brain Behav Immun.* 2017;59:313–21.
64. Nguyen PT, Dorman LC, Pan S, Vainchtein ID, Han RT, Nakao-Inoue H, et al. Microglial remodeling of the extracellular matrix promotes synapse plasticity. *Cell.* 2020;182(2):388–403.e15.
65. Zhang J, Rong P, Zhang L, He H, Zhou T, Fan Y, et al. IL4-driven microglia modulate stress resilience through BDNF-dependent neurogenesis. *Sci Adv.* 2021;7(12):eabb9888.

66. Wang C, Yue H, Hu Z, Shen Y, Ma J, Li J, et al. Microglia mediate forgetting via complement-dependent synaptic elimination. *Science*. 2020;367(6478):688–94.
67. Miyamoto A, Wake H, Ishikawa AW, Eto K, Shibata K, Murakoshi H, et al. Microglia contact induces synapse formation in developing somatosensory cortex. *Nat Commun*. 2016;7:12540.
68. Morris A. Anxiety-induced weight loss. *Nat Rev Endocrinol*. 2019;15(3):130.
69. Ramikie TS, Ressler KJ. Mechanisms of sex differences in fear and posttraumatic stress disorder. *Biol Psychiatry*. 2018;83(10):876–85.
70. Cisternas CD, Cortes LR, Bruggeman EC, Yao B, Forger NG. Developmental changes and sex differences in DNA methylation and demethylation in hypothalamic regions of the mouse brain. *Epigenetics*. 2020;15(1–2):72–84.

## SUPPORTING INFORMATION

Additional supporting information may be found in the online version of the article at the publisher's website.

**How to cite this article:** Fan B-F, Hao B, Dai Y-D, Xue L, Shi Y-W, Liu L, et al. Deficiency of Tet3 in nucleus accumbens enhances fear generalization and anxiety-like behaviors in mice. *Brain Pathology*. 2022;32(6):e13080. <https://doi.org/10.1111/bpa.13080>